Prone position decreases acute lung inflammation measured by [11C](R)-PK11195 positron emission tomography in experimental acute respiratory distress syndrome

François Dhelft, Sophie Lancelot, William Mouton, Didier Le Bars, Nicolas Costes, Emmanuel Roux, Maciej Orkisz, Nazim Benzerdjeb, Jean-Christophe Richard, Laurent Bitker

TITLE PAGE

Title: Prone position decreases acute lung inflammation measured by [^{11}C](R)-PK11195 positron emission tomography in experimental acute respiratory distress syndrome

Authors: François Dhelft[1,2,3], Sophie Lancelot[3,4,5], William Mouton[6], Didier Le Bars[3,4,5], Nicolas Costes[3,4], Emmanuel Roux[2], Maciej Orkisz[2], Nazim Benzerdjeb[7], Jean-Christophe Richard[1,2,3], Laurent Bitker[1,2,3]

Affiliations:

1. Service de Médecine Intensive – Réanimation, Hôpital de la Croix Rousse, Hospices Civils de Lyon, Lyon, France
2. Univ Lyon, INSA-Lyon, Université Claude Bernard Lyon 1, CNRS, Inserm, CREATIS UMR 5220, U1294, Villeurbanne, France
3. Université Lyon 1 Claude Bernard, Lyon, France
4. CERMEP – Imagerie du Vivant, Lyon, France
5. Hospices Civils de Lyon, Lyon, France
6. Laboratoire Commun de Recherche Hospices Civils de Lyon / bioMérieux, Centre Hospitalier Lyon Sud, Hospices Civils de Lyon, France
7. Centre d'Anatomie et Cytologie Pathologique, Centre Hospitalier Lyon Sud, Hospices Civils de Lyon, Lyon, France

Running head: Prone position decreases acute lung inflammation

Correspondence: Dr Laurent Bitker
Service de Médecine Intensive – Réanimation, Hôpital de la Croix Rousse
103, Grande Rue de la Croix Rousse, 69317 Lyon Cedex 04
Mail : laurent.bitker@chu-lyon.fr
ORCID: orcid.org/0000-0002-4698-053X

Manuscript word count: 4427

New & Noteworthy Prone position decreases acute lung macrophage inflammation quantified *in vivo* with [^{11}C](R)-PK11195 positron emission tomography in an experimental

acute respiratory distress syndrome. Regional macrophage inflammation is maximal in the most anterior and posterior lung section of supine animals, in relation with increased regional tidal strain and hyperinflation, and reduced regional lung compliance.

ABSTRACT

Whether prone positioning (PP) modulates acute lung inflammation by the modulation of biomechanical forces of ventilator-induced lung injuries (VILI) remains unclear. We aimed to demonstrate that PP decreases acute lung inflammation in animals with experimental ARDS. Animals were under general anesthesia and protective ventilation (tidal volume 6 $ml.kg^{-1}$, PEEP 5 cmH_2O). ARDS was induced by intra-tracheal instillation of chlorohydric acid. Animals were then randomized to PP, or to supine position (SP). After 4h, a positron emission tomography (PET) acquisition with [^{11}C](R)-PK11195 was performed coupled with computerized tomography (CT) acquisitions, allowing the CT quantification of VILI-associated parameters. [^{11}C](R)-PK11195 lung uptake was quantified using pharmacokinetic multicompartment models. Analyses were performed on 8 lung sections distributed along the antero-posterior dimension. Six animals were randomized to PP, 5 to SP (median P_aO_2/F_iO_2 [interquartile range]: 164 [102–269] mmHg). The normally aerated compartment was significantly redistributed to the posterior lung regions of animals in PP, compared to SP. Dynamic strain was significantly increased in posterior regions of SP animals, compared to PP. After 4h, animals in PP had a significantly lower uptake of [^{11}C](R)-PK11195, compared to SP. [^{11}C](R)-PK11195 regional uptake was independently associated with the study group, dynamic strain, tidal hyperinflation and regional respiratory system compliance in multivariate analysis. In an experimental model of ARDS, 4h of PP significantly decreased acute lung inflammation assessed with PET. The beneficial impact of PP on acute lung inflammation was consecutive to the combination of decreased biomechanical forces and changes in the respiratory system mechanics.

Keywords: acute respiratory distress syndrome, [^{11}C](R)-PK11195, ventilator-induced lung injury, prone position, positron emission tomography

INTRODUCTION

Prone positioning (PP) significantly improves the survival of patients with severe to moderately severe acute respiratory distress syndrome (ARDS). It improves ventilation-perfusion mismatch, oxygenation, alveolar recruitment, and homogenizes the distribution of lung histologic damage (6, 15, 40, 41). PP also alters the chest wall compliance and may decrease ventilator-induced lung injuries (VILI) by uniformizing ventilation distribution throughout lung regions (30, 42, 46). Yet, it remains uncertain whether this modification in regional lung mechanics would translate into a modulation of the ventilator-induced lung inflammatory response (34).

Positron emission tomography (PET) with [^{11}C](R)-PK11195 allows the non-invasive quantification of the translocator protein (TSPO), a mitochondrial receptor expressed by macrophages (26). [^{11}C](R)-PK11195 lung PET can quantify *in vivo* acute lung inflammation triggered by injurious ventilation in swine, using a multiple tissue-compartment kinetic model describing its specific lung uptake (4, 5). Coupled with quantitative lung computerized tomography (CT), [^{11}C](R)-PK11195 lung PET may help identify which biomechanical forces are associated with an increased lung inflammatory response.

We hypothesized that PP would decrease acute lung macrophagic inflammation in animals with experimental ARDS, in relation with regional changes in lung aeration and ventilation. The main objective of the study was to evaluate the impact of PP on lung inflammation assessed *in vivo* by the regional lung uptake of [^{11}C](R)-PK11195 in animals with experimental ARDS.

MATERIAL AND METHODS

Animal conditioning

The protocol was approved by an animal ethics committee (CELYNE, reference 2015041015179195), in accordance with the declaration of Helsinki. Female pigs breeeded and hosted in the same animal facility and weighting 28 [25–30] kg at time of experiment, underwent surgical preparation under mechanical ventilation, continuous general anesthesia (*propofol* 7 $mg.kg^{-1}.h^{-1}$ and *fentanyl* 4 $\mu g.kg^{-1}.h^{-1}$) and neuromuscular blockade (*cisatracrium* 1 $mg.kg^{-1}.h^{-1}$), after prior intramuscular bolus premedication with *xylazine* 0.7 $mg.kg^{-1}$, *ketamine* 2 $mg.kg^{-1}$ and *droperidol* 0.2 $mg.kg^{-1}$.

The tracheal tube was introduced *via* median surgical tracheotomy, secured hermetically and connected to an eXtend ventilator (Taema, Air Liquide, France). Drugs and radiotracer were injected using a central venous catheter surgically hosted in the right internal jugular vein. The animals were also equipped with an arterial catheter placed in the left carotid artery for hemodynamic monitoring, and a pulmonary artery catheter placed in the right jugular vein used to measure the PET radiotracer input function. An esophageal balloon (Marquat Gbm, France) allowed monitoring of esophageal pressures (P_{ES}). Its proper position and adequate non-stress volume were confirmed by the presence of cardiac artifacts, adequate correlation (1±0.2 slope) of airway pressure (P_{AW}) to esophageal pressure (P_{ES}) during an occlusion test, and the absence of P_{ES} changes during epigastric compressions (44, 52).

Experimental protocol

The protocol is summarized in **Figure 1**. Immediately after animal conditioning (T1), we applied protective ventilation in the supine position (SP) using the following settings: tidal

volume (V_T) 6 ml.kg^{-1}, external positive end-expiratory pressure (PEEP) 5 cmH_2O, respiratory rate 25 breaths.min^{-1}, 1:2 inspiratory/expiratory ratio, constant inspiratory flow, and 0.21 O_2 inspired fraction (F_iO_2) (47). Experimental ARDS was induced 1h after the end of animal conditioning, by the intra-tracheal instillation of 0.1 M chlorohydric acid (body weight dose 3 ml.kg^{-1}), possibly followed by an additional 2 ml.kg^{-1} dose if the ratio of arterial O_2 partial pressure (P_aO_2) to F_iO_2 remained > 300 mm Hg (28). Experimental ARDS was confirmed using a P_aO_2/F_iO_2 ratio ≤ 300 mmHg after a 30-min stabilization period (T2). Arterial blood gas were analyzed on a ABL800 FLEX analyzer (Radiometer, France). Once experimental ARDS was achieved, animals were randomized to be placed in PP during 4 hours (T3), or to remain in SP, using a pre-determined random list. Mechanical ventilation settings were left unchanged throughout the protocol (including during imaging procedures), except for a F_iO_2 increase after ARDS onset.

Respiratory mechanics

All airway (P_{AW}) and esophageal (P_{ES}) pressures and gas flow were acquired and analyzed with the Acqknowledge® software (Biopac Systems, CA, USA). Respiratory rate, V_T, total PEEP ($P_{AW,EE}$), airway plateau pressure ($P_{AW,EI}$) and esophageal pressures were repeatedly measured throughout the protocol. $P_{AW,EE}$ and end-expiratory P_{ES} ($P_{ES,EE}$) were measured at the end of a 3-sec expiratory pause, and $P_{AW,EI}$ and end-inspiratory P_{ES} ($P_{ES,EI}$) at the end of a 3-sec inspiratory pause (1). From these, we calculated the difference in end-inspiratory and end-expiratory airway and esophageal pressures (ΔP_{AW} and ΔP_{ES}), respectively. Dividing ΔP_{AW}, ΔP_{ES} and the difference between them by V_T, we obtained the respiratory system elastance (El_{RS}), chest wall elastance (El_{CW}), and lung elastance (El_L), respectively. Lung end-inspiratory transpulmonary driving pressures $P_{L,EI}$ were estimated

using the ratio of El_L to El_{RS} (19). The dynamic and static constituents of elastic mechanical power were also computed (17).

PET/CT imaging protocol

Three sets of CT scans were acquired using a BioGraph TruePoint® PET/CT camera (Siemens, Munich, Germany): before experimental ARDS (T1), after the ARDS stabilization period (T2), and 4 hours later (T3). Each set comprised 3 CT scans: at end-expiration, at end-inspiration, and after transient disconnection from the ventilator (i.e. at functional residual capacity [FRC]). End-expiration and end-inspiration CTs were performed by hermetically clamping of the tracheal tube with 2 Kocher clamps. Longitudinal field-of-view (FOV) extended from the caudal lung extremity to the lung apex. CT settings were as follows: voltage 120 keV, intensity 66 mAs, pitch 0.8, FOV diameter 780 mm, image reconstruction with a B31f smooth filter, slice thickness 2 mm, matrix size 512×512, and pixel size 1.52×1.52 mm.

Lung regions of interest (ROIs) were drawn on all CT scans, using OsiriX (Pixmeo SARL, Bernex, Switzerland), excluding intrathoracic large vessels, large airways, bullae and pneumothorax (13). Then, 10 lung levels were defined by dividing the lung ROI in 10 regions of equal thickness along the antero-posterior axis (**Figure 2**); the 2 most extreme lung levels (#1 and #10) were excluded to avoid small-volume ROIs, resulting in 8 lung levels for regional CT analysis.

Quantitative lung CT analysis

Aeration and CT volumes were computed using MatLab (Natick, Massachusetts, USA) on the whole lung and in the 8 lung levels, using the voxel CT number in Hounsfield units (HU), to estimate voxel gas fraction (16). ROI lung weight was estimated by the product of

150 the ROI volume by its non-gas fraction, assuming a lung tissue density of 1. Four lung
151 aeration compartments were identified on end-expiratory CTs [nonaerated (-100 to +100
152 HU), poorly aerated (-500 to -101 HU), normally aerated (-900 to -501 HU), and hyperinflated
153 (-1000 to -901 HU)] (45). The regional gas volume at end-expiration (EELV), end-inspiration
154 (EILV), and at FRC (V_{FRC}) corresponded to the ROI volume multiplied by its gas fraction (14).
155 Lung inhomogeneity index was calculated at voxel level as the highest ratio of the
156 surrounding voxels' gas fraction to the studied voxel's gas fraction at end-expiration, after
157 gaussian filtering with a radius corresponding to the swine acinus size (9, 10). Their extent
158 corresponded to the fraction of voxels with an inhomogeneity index > 1.685 (10).

159 CT-derived V_T ($V_{T,CT}$) and PEEP-related gas volume (V_{PEEP}) corresponded to the
160 difference between EILV and EELV, and EELV and V_{FRC}, respectively. Tidal lung recruitment
161 and PEEP-related lung recruitment were calculated as the change in non-aerated
162 compartment weight induced by V_T and PEEP and corrected by the end-inspiration and end-
163 expiration gas fractions, respectively (35). Tidal hyperinflation was computed as the
164 difference in hyperinflated volume at end-inspiration and end-expiration. Dynamic strain
165 was computed as the ratio of $V_{T,CT}$ to EELV, and static strain as the ratio of V_{PEEP} to V_{FRC},
166 corrected for tidal and PEEP recruitment, respectively (4). Finally, regional respiratory
167 system compliance (C_{RS}) corresponded to the ratio of regional $V_{T,CT}$ to ΔP_{AW}.

168 *[^{11}C](R)-PK11195 PET acquisition protocol*

169 A [^{11}C](R)-PK11195 PET acquisition was performed at T3 in all animals. The 216-mm
170 longitudinal FOV extended from the caudal lung extremity to its apex. PET acquisitions lasted
171 60 min, starting at the onset of the [^{11}C](R)-PK11195 bolus injection (body weight dose of 6.3
172 [5.3–7.0] MBq.kg^{-1}) on the central venous line. PET frames were reconstructed in 3D

volumes of 112 slices (thickness 2 mm) and 128×128 matrices (2.1×2.1 mm pixel size), as a dynamic series of 18 frames (5×12 sec, 4×60 sec, 7×300 sec, and 2×600 sec). Data were corrected for random coincidences, attenuation, scatter, and ^{11}C isotope decay. ROI masks were drawn on the transmission CT as described above, allowing the acquisition of regional PET time-activity curves (TAC) using MatLab (Natick, MA, USA).

Quantification of [^{11}C](R)-PK11195 lung uptake and study primary outcome

[^{11}C](R)-PK11195 lung uptake was quantified using a 2-tissue-compartment (2TCM) and a 3-tissue-compartment kinetic model (3TCM), as previously described. The 3TCM improves the specific quantification of [^{11}C](R)-PK11195, as it involves a non-specific and irreversible compartment in which the tracer may be trapped (23). The models' output was the non-displaceable binding potential of [^{11}C](R)-PK11195 (BP_{ND}), defined as the ratio of specifically bound [^{11}C](R)-PK11195 to its non-displaceable tissue concentration at equilibrium (25). BP_{ND} reflects the number of TSPO receptors in the lung tissue, and directly quantifies macrophage count. Regional BP_{ND} was the study primary outcome measure, and was calculated as the ratio of the k_3 rate constant, representing [^{11}C](R)-PK11195 binding to the TSPO receptor, to the k_4 rate constant, corresponding to its dissociation from its receptor. Of note, BP_{ND} was not corrected for the ROI tissue fraction, as the k_3/k_4 ratio relates to the bidirectional transfer between the bound compartment and the free compartment, both being contained in the same tissue region (the tissue fraction correction being hence applied on both side of the fraction) (25). We have previously demonstrated that BP_{ND} is unaffected by varying tissue fraction values in lungs with or without experimental ARDS (5).

A summary of PET methodology is presented here (5). In each ROI, resolution of both models (2TCM and 3TCM) was performed using the parent plasma non-invasive input function $C_{PK}(t)$, and the lung ROI TAC $C_{ROI}(t)$ as input data, by means of convolution and weighted non-linear least-square resolution. To select which model best described the lung TAC of a ROI, we applied a 2-step model selection algorithm which led to the determination of ROI's BP_{ND} value (5). $C_{PK}(t)$ was the whole blood radioactivity measured in the pulmonary artery on PET images, corrected for spill-over, partial volume, plasma fraction, metabolite fraction, and regional tissue arrival delay, as previously described (5, 27, 43, 49). The 3TCM model required the determination of F_{WB} (the fraction of blood volume in the ROI) and five rate constants K_1, k_2, k_3, k_4 and k_5 which are: the entry rate constant from blood to tissue, (K_1, corrected for the ROI tissue fraction, and expressed in ml of plasma.min^{-1}.g^{-1} of lung), the backward rate constant of transfer from tissue to blood (k_2 in min^{-1}), the rate constant representing [^{11}C](R)-PK11195 binding to the TSPO receptor (k_3 in min^{-1}), the rate constant corresponding to its dissociation from its receptor (k_4 in min^{-1}), and the rate constant of irreversible uptake by the non-specific compartment (k_5 in min^{-1}) (5, 24). The 2TCM was similar to the 3TCM, with the exception of the non-specific irreversible compartment.

Pathology protocol

After the PET acquisition, animals were euthanized by the intravenous injection of 180 mg.kg^{-1} of *pentobarbital* followed by the disconnection from the ventilator. The right lung and left lung were divided into an anterior region and a posterior region. In each region of each lung, 2 samples of a cubic centimeter were sampled in the cephalic and caudal tiers of the region, respectively (resulting in 4 samples per animal and per lung). Samples of the right lung were prepared for pathology analysis with hematoxylin and eosin staining. Macrophage

presence and histologic lung injury were evaluated on the right lung samples using published semi-quantitative scores by a pathologist blinded to study protocol (4, 6).

Nanostring mRNA multiplex assay

Lungs samples of the left lung were snap frozen in liquid nitrogen and kept at -80° for long-term storage. The whole tissue samples were then placed on an optical coherence tomography compound to make fifty 20 µm frozen sections using a cryostat (Leica Biosystems CM3050S, Wetzlar, Germany). Total RNA from frozen sections was extracted using the RNeasy Blood Mini Kit (Qiagen, Hilden, Germany) according to the manufacturer's instructions. RNA quantity and quality were determined using Nanodrop (Thermofisher Scientific, MA, USA).

The NanoString nCounter® technology (NanoString Technologies, Seattle, WA, USA), a hybridization-based multiplex assay characterized by its amplification-free step, was used for mRNA detection of a multigene custom panel designed with genes known to be crucial to the macrophages/neutrophils immune response (18). The panel included 5 mRNAs of interest [i.e., TSPO, the target of [^{11}C](R)-PK11195 (accession number NM_213753.1), CD68, a protein expressed on the surface of monocytes and macrophages (NM_001291776.1), FCGR3A/B (CD16a/b), a mRNA produced by natural killer cells and neutrophils (NM_214391.2), CD84, a protein expressed on the surface of M1 macrophages (XM_001928464.6), and CD163, a protein expressed on the surface of M2 macrophages (NM_213976.1)] and 3 housekeeping mRNAs [i.e., TBP (XM_013991786.1), SDHA (XM_021076930.1) and RPL4 (XM_005659862.2)] (2, 3). Due to the limited availability of multiplex assays, we randomly selected 36 lung samples among the 44 lung samples collected during the study to perform the analysis.

241 According to manufacturer's instructions, 100 ng of RNA were hybridized to the probes
242 at 67°C for 18 hours using a thermocycler. After removal of excessive probes, samples were
243 loaded into the nCounter Prep Station (NanoString Technologies, Seattle, WA, USA) for
244 purification and immobilization onto the internal surface of a sample cartridge for 2-3 hours.
245 The sample cartridge was then transferred and imaged on the nCounter Digital Analyzer
246 (NanoString Technologies, Seattle, WA, USA) where color codes were counted and tabulated
247 for the selected genes. Data treatment and normalization were next performed using
248 nSolver analysis software (version 4.0, NanoString technologies, Seattle, WA, USA). Each
249 sample was analyzed in a separate multiplexed reaction, each including 8 negative probes
250 and 6 serial concentrations of positive control probes. Negative control analysis was
251 performed to determine the background for each sample. A first step of normalization using
252 the internal positive controls allowed correction of a potential source of variation associated
253 with the technical platform. To do so, we calculated for all samples the background level as
254 the median +3 SD across the six negative probe counts (obtained threshold: 20). Every
255 sample under the background level was fixed to this value. Next, we calculated for each
256 sample the geometric mean of the positive probe counts. The scaling factor for a sample was
257 the ratio of the geometric mean of the sample and the average across all geometric means.
258 For each sample, we divided all gene counts by the corresponding scaling factor. To
259 normalize for differences in RNA input we used the same method as in the positive control
260 normalization, except that geometric means were calculated over the 3 housekeeping genes.
261 Finally, to represent the balance between M1 and M2 macrophage phenotypes, we
262 calculated the ratio of CD84 normalized count to CD68 normalized count, and the CD163
263 normalized count to CD68 normalized count, respectively (51).

Statistics

A *p* value below 0.05 was chosen for statistical significance. All analyses were performed using R (38). All quantitative variables are reported using median and interquartile range in brackets. Comparison of whole lung measurements over time and between groups was performed using mixed effects linear regression, with the animal number as random effect. Association of lung levels (including a quadratic factor) and study group with aeration compartments, CT parameters and regional BP_{ND} were performed using mixed effects regression models, using the lung level and the animal number as random slope within a random intercept (8). Interactions were systematically evaluated. We also performed a multivariate analysis of the CT parameters associated with regional BP_{ND}, using the variables with a *p* value ≤ 0.20 in univariate analysis, and the same random effects as above. Model selection and reduction was performed using backward stepwise selection.

RESULTS

Effect of experimental ARDS

Twelve pigs were included; $P_{AW,EI}$ significantly increased up to 22 [20–24] cmH_2O after ARDS induction (T2) (**Table 1**). P_aO_2/F_iO_2 ratio was non significantly lower in PP vs. SP animals (99 [89–135] vs. 192 [155–225] mmHg, p=0.22) at T2. Between T1 and T2, there was a significant drop in whole lung EELV, and a significant increase in whole lung tissue weight in both groups (**Table 2**). After ARDS induction, 6 animals were randomized to be placed in PP after T2, the rest was left in SP (n=5). One animal in the SP group was excluded due to PET acquisition failure at T3.

Effect of PP on CT parameters and histology

At T3, animals in PP had significantly lower $P_{AW,EI}$, EI_L, and non-aerated lung volume compared to the SP group (**Table 1** and **2**). There was a significant decrease in the regional non-aerated compartment at end-expiration in the posterior lung levels of PP animals (**Figure 3**), and a consecutive EELV redistribution towards posterior regions in this group (**Figure 4**). Regional $V_{T,CT}$ and V_{PEEP} were significantly increased in the anterior regions of SP animals. Also, dynamic strain and lung inhomogeneity index were significantly increased, and regional C_{RS} significantly decreased, in posterior regions of SP animals, compared to PP animals (**Figure 4**).

Histology showed moderate lung injury with significantly higher scores in the posterior regions of both groups, while macrophage recruitment was significantly higher in anterior lung regions of SP animals, compared to PP (**Figure 5**, panels D and E). mRNA quantification showed a significant increase in TSPO expression as well as increased FCGR3A/B expression in SP animals, with a shift towards a M2 macrophage phenotype in the PP group (**Figure 5**).

Effect of PP of [^{11}C](R)-PK11195 lung uptake at T3

Whole lung BP_{ND} reached 0.43 [0.25–0.99] in SP animals, and 0.17 [0.08–0.49] in PP animals. Regional BP_{ND} was significantly increased in all lung levels of SP animals after 4 hours, compared to the PP group (**Figure 6**), with no significant between-group differences in other kinetic-model estimated parameters (**Figure 7**). The antero-posterior distribution of BP_{ND} in SP animals followed a U-shape pattern, with the highest values in the most anterior and posterior lung sections.

Regional [^{11}C](R)-PK11195 BP_{ND} was significantly higher in posterior lung regions of SP animals in relation with higher dynamic strain, and lower regional C_{RS} (**Figure 8**). Anterior

regions of SP animals demonstrated higher EELV and V_{PEEP}, in relation with higher BP_{ND}, compared to PP. Multivariate analysis identified SP group (vs. PP), decreasing regional C_{RS}, and increasing regional dynamic strain and tidal hyperinflation as being positively associated with regional BP_{ND} (**Table 3**).

DISCUSSION

In the present study, we evaluated the effects of PP on acute lung inflammation assessed by the lung uptake of [^{11}C](R)-PK11195 in an animal model of ARDS under protective ventilation. We demonstrated that 1- PP improved regional aeration homogeneity and attenuated VILI biomechanical forces along the antero-posterior axis; 2- under identical protective ventilation strategies, PP significantly attenuated the inflammatory lung response in all lung regions, with maximal effect in the most anterior and posterior lung regions, compared to SP; 3- increased regional inflammation occurred in relation with higher dynamic strain and tidal hyperinflation on the one hand, and deteriorated regional C_{RS} and the body position itself on the other.

Our work is the first to demonstrate *in vivo* that PP modulates regional lung inflammation. We used a widely used, macrophage-specific, PET radiotracer and advanced analytical methodology to ensure its specificity in the study of the inflammatory response to ventilation (5). We observed that lung inflammation was predominant in the posterior and anterior lung regions of SP animals. We observed that this increase in lung macrophage recruitment occurred only 4 hours after ARDS induction despite protective settings. Furthermore, quantitative pathology assays confirmed the increase in TSPO expression in animals maintained in the supine position. These results suggest that conventional ventilator

settings alone do not prevent biomechanical damage and support the use of PP combined with further optimization of mechanical ventilation.

To produce experimental ARDS, we used intratracheal instillation of chlorohydric acid (28, 29). This model is widely considered as a potent model to reproduce direct epithelium damage observed during gastric content aspiration. The model also impacts the endothelium and produces injury proportional to the administered dose of acid. From a pathology point of view, this model implies major neutrophil recruitment, alveolar hemorrhage, fall in lung compliance and FRC. It is considered as a good model to test ventilatory strategies (29). Another advantage is that the model is considered less recruitable than other model such oleic acid or saline lavage.

The mechanisms by which macrophages are recruited in the context of VILI has long been suspected of being secondary to excessive mechanical tidal forces applied to the lung parenchyma (12, 22, 48). Here, we showed that macrophage recruitment is increased in relation with increased dynamic strain and tidal hyperinflation. Dynamic strain was at the highest in the posterior regions of SP animals, in relation with the important loss of aeration that these regions exhibited (32, 39). PP prevented high regional strains in posterior regions efficiently (36). We also observed that dynamic strain increased lung inflammation at levels that were relatively low, compared to previously published data in healthy lungs subjected to high volume ventilation (37). On the other hand, the values associated with increased inflammation were within the range of strain identified by Motta Ribeiro et al. when exploring strain's relationship with metabolic activity in experimental ARDS (32). The underlying assumption is that locally applied dynamic strain may trigger physical damage and inflammation although globally measured strain remains low.

353 Likewise, we observed a significant relationship between macrophagic inflammation
354 and tidal hyperinflation. Tidal hyperinflation is observed in one third of human cases of ARDS
355 and is significantly associated with mortality when its volume exceeds 30% of tidal volume
356 (7, 45). Tidal hyperinflation absolute values were low in our study, and may not have
357 represented the true alveolar volume subjected to overdistension. This may be explained by
358 the fact that hyperinflation is commonly defined by an absolute CT density threshold, whose
359 validity has never been challenged, and may be species-specific (11, 16). It is hence plausible
360 that the phenomenon of tidal hyperinflation may be of greater magnitude if higher HU
361 threshold were used. Also, tidal hyperinflation may be the consequence of excessive tidal
362 excursion applied to regions with low aerated volumes at end-expiration at low PEEP (baby
363 lung), or on the contrary appear in case of large normally aerated compartments secondary
364 to high PEEP (33).
365 We also found that lung regions with lower C_{RS} demonstrated lower lung [^{11}C](R)-
366 PK11195 BP_{ND}, implying that not only do tidal forces exert mechanical stress with secondary
367 biotrauma, but also that they do it in combination with the intrinsic alteration of the lung
368 elastic characteristics. This is congruent with our findings of higher inflammation in the
369 posterior regions of SP animals, where the initial experimental hit was predominantly
370 distributed, accompanied with loss of aeration, increase in the non-aerated lung fraction and
371 greater lung inhomogeneity indices.
372 The supine position was identified as one of the independent factors associated with
373 lung inflammation in multivariate analysis. We hypothesize that this factor alone could
374 explain the increase in BP_{ND} observed in anterior lung sections, when other CT parameters
375 could not. However, we cannot exclude that the effect of the intervention on lung
376 inflammation was not only mediated by its impact on lung recruitment and homogenization

of ventilation, as stress and strain were not kept constant after proning. Of note, only EELV and V_{PEEP} showed major differences in the anterior regions of SP animals, compared to PP. Although not retained in the final multivariate model, we hypothesize that BP_{ND} was increased in these regions due to the mechanical stress induced by PEEP in relation with the effects of SP on the chest wall (52). Indeed, although all animals were applied the same level of PEEP, animals in SP may have encountered greater regional transpulmonary pressures due to higher antero-posterior gradient of pleural pressures in SP, and larger ventilation of the non-dependent "baby lung" (44, 46, 52). This is also suggested by the fact that regional C_{RS} was not significantly different in anterior lung regions, meaning that if the volume was kept constant and pleural pressures decrease in SP compared to PP, transpulmonary pressures must have been higher in these regions. Of note, this mechanism of injury is not identified by static strain at conventional ventilation regimens, as both the resting volume and its variation increased proportionally when lung elastance is kept constant. Finally, it is possible that the regional distribution of acute lung injury by HCl administration may have been impacted by proning despite the 30 minutes stabilization period (31). Although this period of time is usually deemed sufficient to stabilize injury, proning may have decreased the regional effect of the acid.

Our results imply two therapeutic assumptions. First, homogenization of lung aeration and regional ventilation remains an important target in ARDS management. PP allows such a decrease in the biomechanical forces of VILI, that would otherwise be applied to posterior regions of subjects in SP. This was made possible without applying higher PEEP levels, which may increase alveolar overdistension and induce hemodynamic impairment, with potentially harmful consequences (50). The second implication of our results is that mechanical ventilation in SP was harmful despite the use of conventional protective ventilation. This also

implies that low PEEP levels may be injurious in normally aerated lungs, when there exist large geospatial heterogeneities in lung injury distribution, as in our model.

Several limitations must be acknowledged. First, we were unable to compare the results of lung BP_{ND} against TSPO quantification in pathology to allow the assessment of the radiotracer's specificity. However, our group has previously published 2 studies showing the association of [^{11}C](R)-PK11195 lung uptake with a semi-quantitative score of lung macrophage recruitment in pathology (4, 5). Second, CT determination of dynamic strain and tidal hyperinflation may have been impacted by registration errors. However, lung distortion was limited in our model, as tidal volumes were kept within the clinical range. Third, BP_{ND} data measured in healthy pigs ventilated in SP or PP has not been acquired, and may have informed on the baseline radiotracer uptake in normal lungs subjected to protective ventilation. Finally, PP was applied for only 4 hours before the primary outcome was evaluated, and we are unable to conclude how longer periods of PP would have impacted regional lung inflammation. Yet, PP should be administered for at least 16 hours or more, as shorter durations may not prove as effective in terms of lung protection, recruitment, and clinical outcome, which let us hypothesize that a similar experiment over an extended period of time (>4 hours) would have potentially resulted in larger effect size (20, 21).

CONCLUSIONS

In an experimental model of ARDS subjected to conventional protective ventilation, PP significantly homogenized regional lung aeration and ventilation, and significantly decreased acute lung macrophagic inflammation quantified in PET, compared to SP. The beneficial impact of PP on acute lung inflammation is the consequence of the combination of

decreased VILI-related biomechanical forces and the alteration of the lung and chest wall intrinsic characteristics induced by the body position.

DECLARATIONS

Acknowledgments

The authors are grateful to Frederic Bonnefoi, Thibaut Iecker, Christian Tourvieille, Franck Lavenne, Jérôme Redouté, and Jean-Baptiste Langlois, all at Centre d'Etude et de Recherche Multimodal et Pluridisciplinaire (CERMEP), for their precious help.

Authors' contributions

FD collected and analyzed the data, interpreted the results, drafted the manuscript. SL collected and analyzed the data, made substantial revisions to the manuscript for important intellectual content. DLB collected and analyzed the data, made substantial revisions to the manuscript for important intellectual content. NC interpreted the data, made substantial revisions to the manuscript for important intellectual content. ER interpreted the data, made substantial revisions to the manuscript for important intellectual content. MO interpreted the data, made substantial revisions to the manuscript for important intellectual content. NB collected, analyzed and interpreted the data, made substantial revisions to the manuscript for important intellectual content. JCR designed the study, collected, analyzed and interpreted the data, made substantial revisions to the manuscript for important intellectual content. LB designed the study, collected, analyzed and interpreted the data, made substantial revisions to the manuscript for important intellectual content. All authors approved the final version of the manuscript, and agree to be accountable for all aspects of the work.

Funding

The present work was funded by a grant of the Société de Réanimation de Langue Française (Bourse de Recherche Expérimentale), and a grant of the Hospices Civils de Lyon (Bourse Jeune Chercheur 2019).

Competing interests

All authors, except one, have declared no conflicts of interest, financial or otherwise. JCR reported study funding by Hamilton Medical (Suisse), unrelated to the present work.

Data availability

Data will be made available upon reasonable request.

Code availability

Code will be made available upon reasonable request.

REFERENCES

1. **Barberis L, Manno E, and Guerin C**. Effect of end-inspiratory pause duration on plateau pressure in mechanically ventilated patients. *Intensive care medicine* 29: 130-134, 2003.
2. **Barros MH, Hauck F, Dreyer JH, Kempkes B, and Niedobitek G**. Macrophage polarisation: an immunohistochemical approach for identifying M1 and M2 macrophages. *PLoS One* 8: e80908, 2013.
3. **Bertrand G, Duprat E, Lefranc MP, Marti J, and Coste J**. Characterization of human FCGR3B*02 (HNA-1b, NA2) cDNAs and IMGT standardized description of FCGR3B alleles. *Tissue Antigens* 64: 119-131, 2004.
4. **Bitker L, Costes N, Le Bars D, Lavenne F, Orkisz M, Hernandez Hoyos M, Benzerdjeb N, Devouassoux M, and Richard JC**. Noninvasive quantification of macrophagic lung recruitment during experimental ventilation-induced lung injury. *J Appl Physiol* 127: 546-558, 2019.
5. **Bitker L, Dhelft F, Lancelot S, Le Bars D, Costes N, Benzerdjeb N, Orkisz M, and Richard JC**. Non-invasive quantification of acute macrophagic lung inflammation with [(11)C](R)-PK11195 using a three-tissue compartment kinetic model in experimental acute respiratory distress syndrome. *Eur J Nucl Med Mol Imaging* 49: 2122-2136, 2022.
6. **Broccard AF, Shapiro RS, Schmitz LL, Ravenscraft SA, and Marini JJ**. Influence of prone position on the extent and distribution of lung injury in a high tidal volume oleic acid model of acute respiratory distress syndrome. *Critical care medicine* 25: 16-27, 1997.
7. **Chauvelot L, Bitker L, Dhelft F, Mezidi M, Orkisz M, Davila Serrano E, Penarrubia L, Yonis H, Chabert P, Folliet L, David G, Provoost J, Lecam P, Boussel L, and Richard JC**. Quantitative-analysis of computed tomography in COVID-19 and non COVID-19 ARDS patients: A case-control study. *J Crit Care* 60: 169-176, 2020.
8. **Cnaan A, Laird NM, and Slasor P**. Using the general linear mixed model to analyse unbalanced repeated measures and longitudinal data. *Stat Med* 16: 2349-2380, 1997.
9. **Cressoni M, Cadringher P, Chiurazzi C, Amini M, Gallazzi E, Marino A, Brioni M, Carlesso E, Chiumello D, Quintel M, Bugedo G, and Gattinoni L**. Lung inhomogeneity in patients with acute respiratory distress syndrome. *Am J Respir Crit Care Med* 189: 149-158, 2014.
10. **Cressoni M, Chiurazzi C, Gotti M, Amini M, Brioni M, Algieri I, Cammaroto A, Rovati C, Massari D, di Castiglione CB, Nikolla K, Montaruli C, Lazzerini M, Dondossola D, Colombo A, Gatti S, Valerio V, Gagliano N, Carlesso E, and Gattinoni L**. Lung inhomogeneities and time course of ventilator-induced mechanical injuries. *Anesthesiology* 123: 618-627, 2015.
11. **Dambrosio M, Roupie E, Mollet JJ, Anglade MC, Vasile N, Lemaire F, and Brochard L**. Effects of positive end-expiratory pressure and different tidal volumes on alveolar recruitment and hyperinflation. *Anesthesiology* 87: 495-503, 1997.
12. **Frank JA, Wray CM, McAuley DF, Schwendener R, and Matthay MA**. Alveolar macrophages contribute to alveolar barrier dysfunction in ventilator-induced lung injury. *Am J Physiol Lung Cell Mol Physiol* 291: L1191-1198, 2006.
13. **Gattinoni L, Caironi P, Cressoni M, Chiumello D, Ranieri VM, Quintel M, Russo S, Patroniti N, Cornejo R, and Bugedo G**. Lung recruitment in patients with the acute respiratory distress syndrome. *N Engl J Med* 354: 1775-1786, 2006.

14. **Gattinoni L, Pelosi P, Crotti S, and Valenza F**. Effects of positive end-expiratory pressure on regional distribution of tidal volume and recruitment in adult respiratory distress syndrome. *Am J Respir Crit Care Med* 151: 1807-1814, 1995.
15. **Gattinoni L, Pelosi P, Vitale G, Pesenti A, D'Andrea L, and Mascheroni D**. Body position changes redistribute lung computed-tomographic density in patients with acute respiratory failure. *Anesthesiology* 74: 15-23, 1991.
16. **Gattinoni L, Pesenti A, Bombino M, Baglioni S, Rivolta M, Rossi F, Rossi G, Fumagalli R, Marcolin R, Mascheroni D, and et al.** Relationships between lung computed tomographic density, gas exchange, and PEEP in acute respiratory failure. *Anesthesiology* 69: 824-832, 1988.
17. **Giosa L, Busana M, Pasticci I, Bonifazi M, Macri MM, Romitti F, Vassalli F, Chiumello D, Quintel M, Marini JJ, and Gattinoni L**. Mechanical power at a glance: a simple surrogate for volume-controlled ventilation. *Intensive Care Med Exp* 7: 61, 2019.
18. **Goytain A, and Ng T**. NanoString nCounter Technology: High-Throughput RNA Validation. *Methods Mol Biol* 2079: 125-139, 2020.
19. **Grieco DL, Chen L, and Brochard L**. Transpulmonary pressure: importance and limits. *Ann Transl Med* 5: 285, 2017.
20. **Guerin C, Gaillard S, Lemasson S, Ayzac L, Girard R, Beuret P, Palmier B, Le QV, Sirodot M, Rosselli S, Cadiergue V, Sainty JM, Barbe P, Combourieu E, Debatty D, Rouffineau J, Ezingeard E, Millet O, Guelon D, Rodriguez L, Martin O, Renault A, Sibille JP, and Kaidomar M**. Effects of systematic prone positioning in hypoxemic acute respiratory failure: a randomized controlled trial. *JAMA* 292: 2379-2387, 2004.
21. **Guerin C, Reignier J, Richard JC, Beuret P, Gacouin A, Boulain T, Mercier E, Badet M, Mercat A, Baudin O, Clavel M, Chatellier D, Jaber S, Rosselli S, Mancebo J, Sirodot M, Hilbert G, Bengler C, Richecoeur J, Gainnier M, Bayle F, Bourdin G, Leray V, Girard R, Baboi L, Ayzac L, and Group PS**. Prone positioning in severe acute respiratory distress syndrome. *N Engl J Med* 368: 2159-2168, 2013.
22. **Hamanaka K, Jian MY, Townsley MI, King JA, Liedtke W, Weber DS, Eyal FG, Clapp MM, and Parker JC**. TRPV4 channels augment macrophage activation and ventilator-induced lung injury. *Am J Physiol Lung Cell Mol Physiol* 299: L353-362, 2010.
23. **Hatty CR, Le Brun AP, Lake V, Clifton LA, Liu GJ, James M, and Banati RB**. Investigating the interactions of the 18kDa translocator protein and its ligand PK11195 in planar lipid bilayers. *Biochim Biophys Acta* 1838: 1019-1030, 2014.
24. **Holman BF, Cuplov V, Millner L, Hutton BF, Maher TM, Groves AM, and Thielemans K**. Improved correction for the tissue fraction effect in lung PET/CT imaging. *Phys Med Biol* 60: 7387-7402, 2015.
25. **Innis RB, Cunningham VJ, Delforge J, Fujita M, Gjedde A, Gunn RN, Holden J, Houle S, Huang SC, Ichise M, Iida H, Ito H, Kimura Y, Koeppe RA, Knudsen GM, Knuuti J, Lammertsma AA, Laruelle M, Logan J, Maguire RP, Mintun MA, Morris ED, Parsey R, Price JC, Slifstein M, Sossi V, Suhara T, Votaw JR, Wong DF, and Carson RE**. Consensus nomenclature for in vivo imaging of reversibly binding radioligands. *J Cereb Blood Flow Metab* 27: 1533-1539, 2007.
26. **Jones HA, Valind SO, Clark IC, Bolden GE, Krausz T, Schofield JB, Boobis AR, and Haslett C**. Kinetics of lung macrophages monitored in vivo following particulate challenge in rabbits. *Toxicol Appl Pharmacol* 183: 46-54, 2002.

27. **Kropholler MA, Boellaard R, Elzinga EH, van der Laken CJ, Maruyama K, Kloet RW, Voskuyl AE, Dijkmans BA, and Lammertsma AA**. Quantification of (R)-[11C]PK11195 binding in rheumatoid arthritis. *Eur J Nucl Med Mol Imaging* 36: 624-631, 2009.
28. **Matute-Bello G, Downey G, Moore BB, Groshong SD, Matthay MA, Slutsky AS, and Kuebler WM**. An official American Thoracic Society workshop report: features and measurements of experimental acute lung injury in animals. *Am J Respir Cell Mol Biol* 44: 725-738, 2011.
29. **Matute-Bello G, Frevert CW, and Martin TR**. Animal models of acute lung injury. *Am J Physiol Lung Cell Mol Physiol* 295: L379-399, 2008.
30. **Mentzelopoulos SD, Roussos C, and Zakynthinos SG**. Prone position reduces lung stress and strain in severe acute respiratory distress syndrome. *Eur Respir J* 25: 534-544, 2005.
31. **Modelska K, Pittet JF, Folkesson HG, Courtney Broaddus V, and Matthay MA**. Acid-induced lung injury. Protective effect of anti-interleukin-8 pretreatment on alveolar epithelial barrier function in rabbits. *Am J Respir Crit Care Med* 160: 1450-1456, 1999.
32. **Motta-Ribeiro GC, Hashimoto S, Winkler T, Baron RM, Grogg K, Paula L, Santos A, Zeng C, Hibbert K, Harris RS, Bajwa E, and Vidal Melo MF**. Deterioration of Regional Lung Strain and Inflammation during Early Lung Injury. *Am J Respir Crit Care Med* 198: 891-902, 2018.
33. **Nieszkowska A, Lu Q, Vieira S, Elman M, Fetita C, and Rouby JJ**. Incidence and regional distribution of lung overinflation during mechanical ventilation with positive end-expiratory pressure. *Critical care medicine* 32: 1496-1503, 2004.
34. **Papazian L, Gainnier M, Marin V, Donati S, Arnal JM, Demory D, Roch A, Forel JM, Bongrand P, Bregeon F, and Sainty JM**. Comparison of prone positioning and high-frequency oscillatory ventilation in patients with acute respiratory distress syndrome. *Critical care medicine* 33: 2162-2171, 2005.
35. **Paula LF, Wellman TJ, Winkler T, Spieth PM, Guldner A, Venegas JG, Gama de Abreu M, Carvalho AR, and Vidal Melo MF**. Regional tidal lung strain in mechanically ventilated normal lungs. *J Appl Physiol* 121: 1335-1347, 2016.
36. **Perchiazzi G, Rylander C, Vena A, Derosa S, Polieri D, Fiore T, Giuliani R, and Hedenstierna G**. Lung regional stress and strain as a function of posture and ventilatory mode. *J Appl Physiol (1985)* 110: 1374-1383, 2011.
37. **Protti A, Cressoni M, Santini A, Langer T, Mietto C, Febres D, Chierichetti M, Coppola S, Conte G, Gatti S, Leopardi O, Masson S, Lombardi L, Lazzerini M, Rampoldi E, Cadringher P, and Gattinoni L**. Lung stress and strain during mechanical ventilation: any safe threshold? *Am J Respir Crit Care Med* 183: 1354-1362, 2011.
38. **R Development Core Team**. R: A language and environment for statistical computing. Vienna, Austria: R Foundation for Statistical Computing, 2008.
39. **Retamal J, Hurtado D, Villarroel N, Bruhn A, Bugedo G, Amato MBP, Costa ELV, Hedenstierna G, Larsson A, and Borges JB**. Does Regional Lung Strain Correlate With Regional Inflammation in Acute Respiratory Distress Syndrome During Nonprotective Ventilation? An Experimental Porcine Study. *Critical care medicine* 46: e591-e599, 2018.
40. **Richard JC, Janier M, Lavenne F, Berthier V, Lebars D, Annat G, Decailliot F, and Guerin C**. Effect of position, nitric oxide, and almitrine on lung perfusion in a porcine model of acute lung injury. *J Appl Physiol (1985)* 93: 2181-2191, 2002.

41. **Richter T, Bellani G, Scott Harris R, Vidal Melo MF, Winkler T, Venegas JG, and Musch G**. Effect of prone position on regional shunt, aeration, and perfusion in experimental acute lung injury. *Am J Respir Crit Care Med* 172: 480-487, 2005.
42. **Santini A, Protti A, Langer T, Comini B, Monti M, Sparacino CC, Dondossola D, and Gattinoni L**. Prone position ameliorates lung elastance and increases functional residual capacity independently from lung recruitment. *Intensive Care Med Exp* 3: 55, 2015.
43. **Schroeder T, Vidal Melo MF, Musch G, Harris RS, Venegas JG, and Winkler T**. Image-derived input function for assessment of 18F-FDG uptake by the inflamed lung. *J Nucl Med* 48: 1889-1896, 2007.
44. **Talmor D, Sarge T, Malhotra A, O'Donnell CR, Ritz R, Lisbon A, Novack V, and Loring SH**. Mechanical ventilation guided by esophageal pressure in acute lung injury. *N Engl J Med* 359: 2095-2104, 2008.
45. **Terragni PP, Rosboch G, Tealdi A, Corno E, Menaldo E, Davini O, Gandini G, Herrmann P, Mascia L, Quintel M, Slutsky AS, Gattinoni L, and Ranieri VM**. Tidal hyperinflation during low tidal volume ventilation in acute respiratory distress syndrome. *Am J Respir Crit Care Med* 175: 160-166, 2007.
46. **Terzi N, Bayat S, Noury N, Turbil E, Habre W, Argaud L, Cour M, Louis B, and Guerin C**. Comparison of pleural and esophageal pressure in supine and prone positions in a porcine model of acute respiratory distress syndrome. *J Appl Physiol (1985)* 128: 1617-1625, 2020.
47. **The Acute Respiratory Distress Syndrome Network**. Ventilation with lower tidal volumes as compared with traditional tidal volumes for acute lung injury and the acute respiratory distress syndrome. *N Engl J Med* 342: 1301-1308, 2000.
48. **Tsuno K, Miura K, Takeya M, Kolobow T, and Morioka T**. Histopathologic pulmonary changes from mechanical ventilation at high peak airway pressures. *Am Rev Respir Dis* 143: 1115-1120, 1991.
49. **Wellman TJ, Winkler T, and Vidal Melo MF**. Modeling of Tracer Transport Delays for Improved Quantification of Regional Pulmonary ^{18}F-FDG Kinetics, Vascular Transit Times, and Perfusion. *Ann Biomed Eng* 43: 2722-2734, 2015.
50. **Writing Group for the Alveolar Recruitment for Acute Respiratory Distress Syndrome Trial I, Cavalcanti AB, Suzumura EA, Laranjeira LN, Paisani DM, Damiani LP, Guimaraes HP, Romano ER, Regenga MM, Taniguchi LNT, Teixeira C, Pinheiro de Oliveira R, Machado FR, Diaz-Quijano FA, Filho MSA, Maia IS, Caser EB, Filho WO, Borges MC, Martins PA, Matsui M, Ospina-Tascon GA, Giancursi TS, Giraldo-Ramirez ND, Vieira SRR, Assef M, Hasan MS, Szczeklik W, Rios F, Amato MBP, Berwanger O, and Ribeiro de Carvalho CR**. Effect of Lung Recruitment and Titrated Positive End-Expiratory Pressure (PEEP) vs Low PEEP on Mortality in Patients With Acute Respiratory Distress Syndrome: A Randomized Clinical Trial. *JAMA* 318: 1335-1345, 2017.
51. **Yang C, Wei C, Wang S, Shi D, Zhang C, Lin X, Dou R, and Xiong B**. Elevated CD163(+)/CD68(+) Ratio at Tumor Invasive Front is Closely Associated with Aggressive Phenotype and Poor Prognosis in Colorectal Cancer. *Int J Biol Sci* 15: 984-998, 2019.
52. **Yoshida T, Amato MBP, Grieco DL, Chen L, Lima CAS, Roldan R, Morais CCA, Gomes S, Costa ELV, Cardoso PFG, Charbonney E, Richard JM, Brochard L, and Kavanagh BP**. Esophageal Manometry and Regional Transpulmonary Pressure in Lung Injury. *Am J Respir Crit Care Med* 197: 1018-1026, 2018.

FIGURE LEGENDS

Figure 1. Study protocol

The figure shows the protocol process, with the 2 main study steps (T1, T2 and T3) according to the corresponding CT acquisitions. CT study designates the 3 CT acquisitions that were performed at end-expiration, end-inspiration and FRC in all animals. PET study designates the [^{11}C](R)-PK11195 60-min PET acquisition that was performed 4 hours after randomization. ARDS designates the time point at which ARDS induction was performed (between T1 and T2). Apart from body position, all animals received the exact same interventions, including ventilatory settings (described on the right-hand side of the figure). After T3, animals were euthanized and samples from the right lung were send in pathology. ARDS: acute respiratory distress syndrome; CT: computerized tomography; FiO_2: inspired fraction in O_2; FRC: functional residual capacity; I:E: ratio of inspiratory time over expiratory time; PEEP: positive end-expiratory pressure; PET: positron emission tomography; RR: respiratory rate; VT: tidal volume

Figure 2. Lung segmentation

The figure shows the 8 lung levels along the antero-posterior axis in an illustrative animal, in the axial view (A, at mid-lung level) and the sagittal view (B, through the right lung).

Figure 3. Aeration compartment distribution in lung levels based on study group at T3

The figure shows the mean fraction of each of the 4 aeration compartments (non-, poorly, normally aerated, and hyperinflated) in each of the 8 lung levels, in animals in the prone and the supine groups, 4 hours after experimental ARDS stabilization (T3). There was a significant association between the distribution of the non-aerated, poorly aerated and

normally aerated fractions and the interaction Group x Level. The # corresponds to a $p<0.05$ in the post-hoc pairwise analysis evaluating the difference in fraction level for a given aeration compartment in the same lung level, between study groups, and accounting for the repetition of tests.

Figure 4. Regional CT parameters in both study groups at T3 (figure is on the preceding page)

The figure shows the values of the end-expiratory aerated lung volume (A), lung weight at end-expiration (B), lung inhomogeneities index (C), lung inhomogeneities extent (D), regional C_{RS} (E), $V_{T,CT}$ (F), tidal recruitment (G), tidal hyperinflation (H), V_{PEEP} (I), PEEP-induced recruitment (J), dynamic strain (K), and static strain (H) in each of the 8 lung levels, in animals in the supine position (red boxplots) and those in the prone position (blue boxplots). Tidal recruitment and hyperinflation are expressed as a percentage of $V_{T,CT}$, and PEEP-related recruitment as relative to V_{PEEP}. The p value examines the association of the studied parameter with interaction of Study Group x Lung Level (including a quadratic factor, if statistically significant). In case of a non-significant interaction term, the p value of the independent effect of Group is given. C_{RS}: respiratory system compliance; PEEP: positive end-expiratory pressure; V_{PEEP}: PEEP-related increase in gas volume, $V_{T,CT}$: computerized tomography-derived tidal volume.

Figure 5. Lung pathology scores and mRNA assays in both study groups

Panels A, B and C show representative pathology slides form 3 lung regions sampled in the same animal. For each sample, the corresponding macrophage score is given. In panels B and C, an inset shows a zoom of the same sample with multiple macrophages (isolated or in clusters, respectively), with the black arrows pointing at macrophages. Panel D shows the mean histologic lung injury score in the 4 lung regions (antero-cephalic, antero-caudal,

postero-cephalic and postero-caudal) of the 2 study groups (SP in red and PP in blue), with individual data represented (6). No difference in the score between study groups was observed; the score was significantly higher the 2 caudal regions, compared to the antero-cephalic region (p<0.05). Panel E shows the mean macrophage recruitment score in the same 4 lung regions of the 2 study groups (SP in red and PP in blue), with individual data represented. The macrophage score was significantly higher between study groups in the antero-cephalic and postero-cephalic regions (§: p<0.05 in the post-hoc pairwise analysis). Panels F to J shows the results of the mRNA multi-gene panel assay performed with the Nanostring technology in the same 4 lung regions, showing the quantity of mRNA (expressed in normalized counts, nc) of TSPO (F), CD68 (G), FCGR3A/B (H), CD84/CD68 ratio (I) and CD163/CD68 ratio (J). The panels show the individual value observed in each region, and corresponding boxplots (SP in red and PP in blue). Ant-caud: antero-caudal; ant-ceph: antero-cephalic; nc: normalized count; post-caud: postero-caudal; post-ceph: postero-cephalic; PP: prone position; SP: supine position; TSPO: translocator protein.

Figure 6. [^{11}C](R)-PK11195 BP_{ND} in each lung level in the 2 study groups at T3

Panel A shows representative BP_{ND} parametric images (determined at voxel level using the same TCM methodology) of an animal in the prone position and of another in the supine position. The color scale describes the voxels BP_{ND} values in PET images. Anatomical level and relationships are given with the black arrow on the left, and the corresponding end-expiratory CT slice. The red box shows lung regions with high macrophagic inflammation, as estimated by the [^{11}C](R)-PK11195 BP_{ND}. Panels B and C show the BP_{ND} of [^{11}C](R)-PK11195 in each of the 8 lung levels, in animals in the supine position (red boxplots, points and lines) and those in the prone position (blue boxplots, points and lines). Panel B shows the

705 experimental data with individual values collected at T3 in all animals. Panel C shows the
706 results of the mixed effects model describing the effect of study group and lung levels on
707 BP_{ND} values (BP_{ND} values were normalized by the random effects determined by the mixed
708 effects regression to improve graphical representation). In panel C, the grey shading
709 represented the 95% confidence interval of the model. The *p* value examines the association
710 between the interaction of study group with lung level (including a quadratic factor), and
711 lung level BP_{ND}. BP_{ND}: non-displaceable binding potential. BP_{ND}: [^{11}C](R)-PK11195 binding
712 potential.

713 *Figure 7. Regional [^{11}C](R)-PK11195 kinetic model parameter estimates at T3*

714 The figure shows the regional K_1 to k_2 ratio (A), blood fraction F_{WB} (B) and k_5 (C) in the 8
715 lung sections in animals in the supine position (red boxplots) and those in the prone position
716 (blue boxplots). The K_1 rate constant was corrected for the ROI tissue fraction and expressed
717 in ml of plasma.min^{-1}.g^{-1} of tissue. The data is presented with boxplots. We evaluated the
718 association of the studied parameter with the interaction of Study Group x Lung Level
719 (including a quadratic factor, if significant). In case of a non-significant interaction term, the
720 *p* value of the independent effect of Group is given. F_{WB}: regional blood fraction.

721 *Figure 8. Regional [^{11}C](R)-PK11195 BP_{ND} in relation with regional CT parameters at T3*

722 The figure shows the regional BP_{ND} as a function of regional C_{RS} (A), lung
723 inhomogeneity index (B), EELV (C), V_{PEEP} (D), dynamic strain (E) and tidal hyperinflation (F).
724 The 3 lung sections are defined as Levels 1-2 for the most anterior lung levels, Levels 3-6 for
725 the mid-lung section, and Levels 7-8 for the most posterior slices. On each plot left side, the
726 values of regional BP_{ND} are summarized using boxplots, separated based on the study group.
727 On the upper part of each plot, we also show the distribution of the variable of interest,

728 separated based on the study group. Blue dots, boxplots and distribution plots corresponds
729 to PP animals, red dots, boxplots, and distribution plots to SP animals. The *p* values given in
730 each plot identify the statistical difference of each variable between study groups in that
731 region, using multiple comparison methodology. Standardized BP_{ND} values are given, using
732 the random effects determined in the multivariate analysis. BP_{ND}: binding potential; C_{RS}:
733 respiratory system compliance; EELV: end-expiratory lung volume; PEEP: positive end-
734 expiratory pressure; V_{PEEP}: PEEP-induced increase in gas volume; PP: prone position; SP:
735 supine position.
736
737

Prone position decreases acute lung inflammation measured with [^{11}C](R)-PK11195 PET in experimental ARDS

METHODS

Randomized controlled preclinical trial of the effect of prone position versus supine position on lung macrophagic inflammation, quantified in PET using the [11C](R)-PK11195 TSPO ligand, in swine with experimental ARDS.

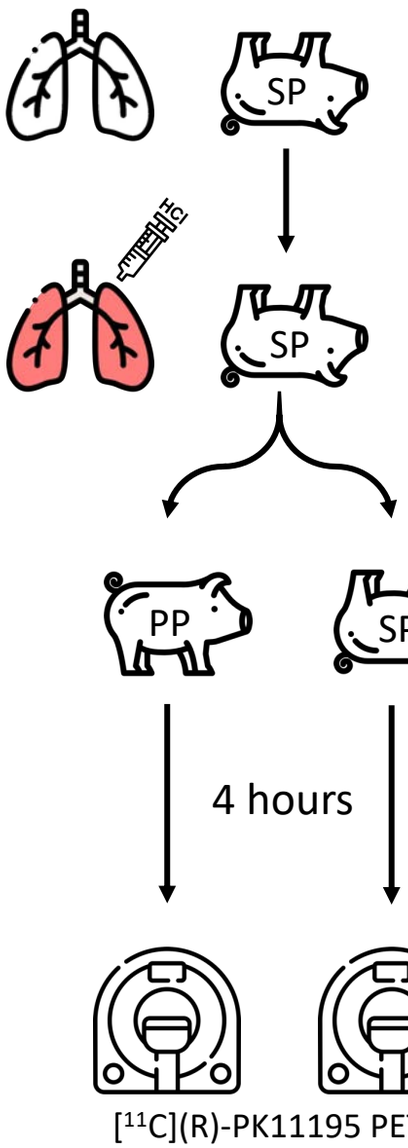

1
- Healthy pigs (30 kg) in the supine position (SP)
- Ventilated with V_T 6 ml.kg^{-1}, PEEP 5 cmH_2O

2
- ARDS induction with intratracheal chlorohydric acid instillation
- Target PaO_2/FiO_2 < 300 mm Hg

3
- Randomization to prone position or to remain in SP
- Ventilator settings unchanged (V_T 6 ml.kg^{-1}, PEEP 5 cmH_2O)
- Position maintained during 4 hours

4
- Regional lung inflammation quantified by the binding potential (BP_{ND}) of [^{11}C](R)-PK11195, determined using multicompartmental pharmacokinetic models.

OUTCOME

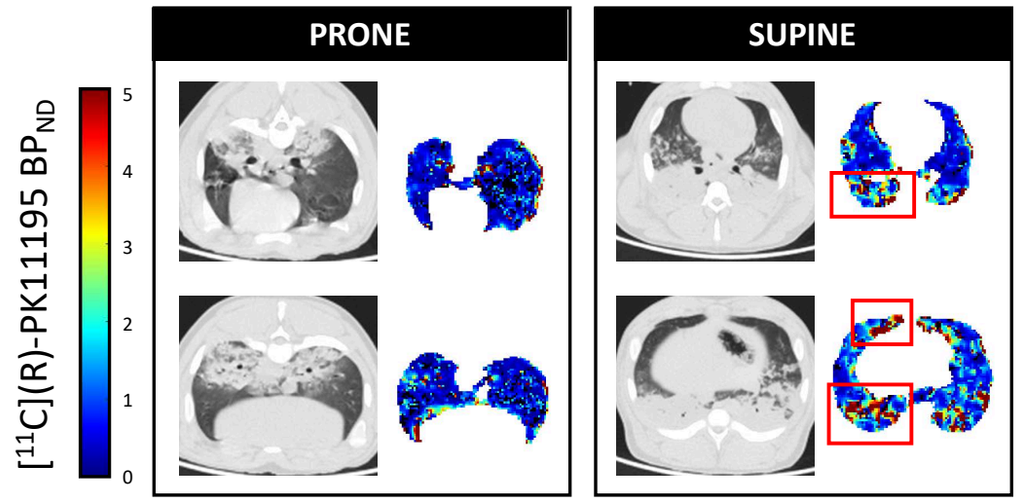

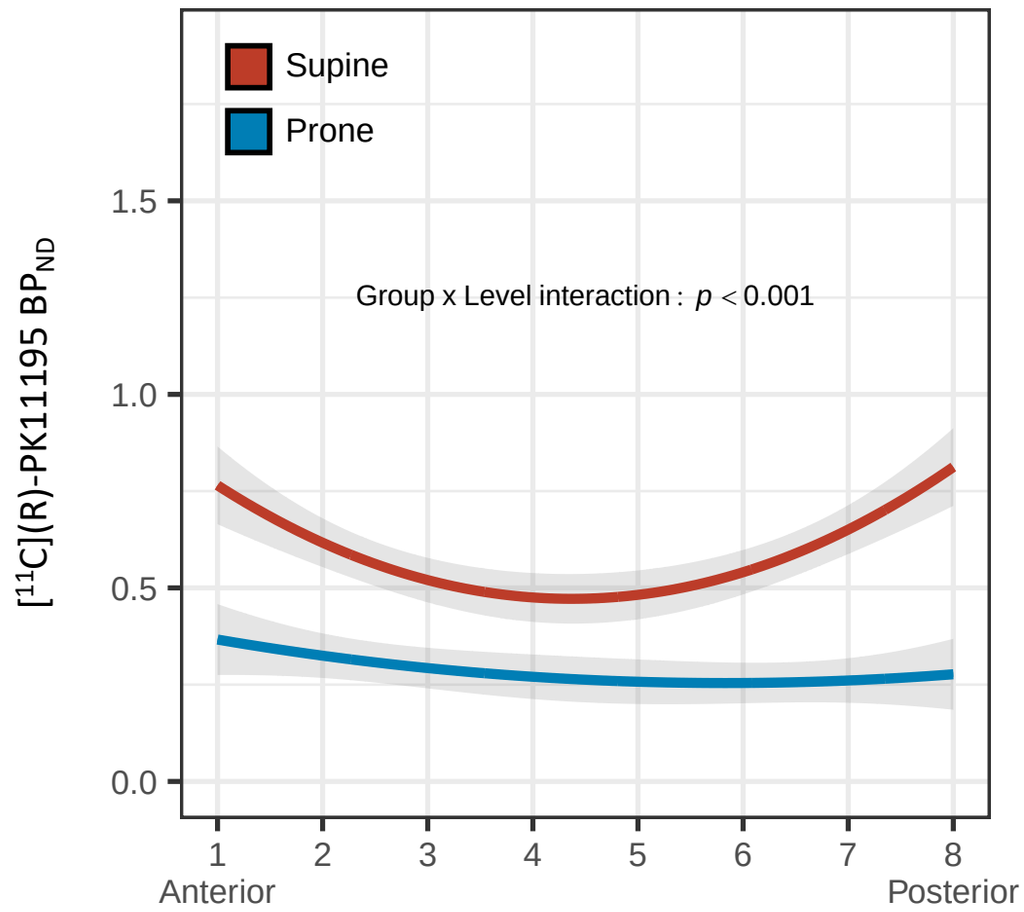

CONCLUSIONS

In an experimental model of ARDS, 4h of prone positioning significantly decreased acute lung inflammation in all lung regions, consecutive to decreased biomechanical forces and changes in the respiratory system mechanics.

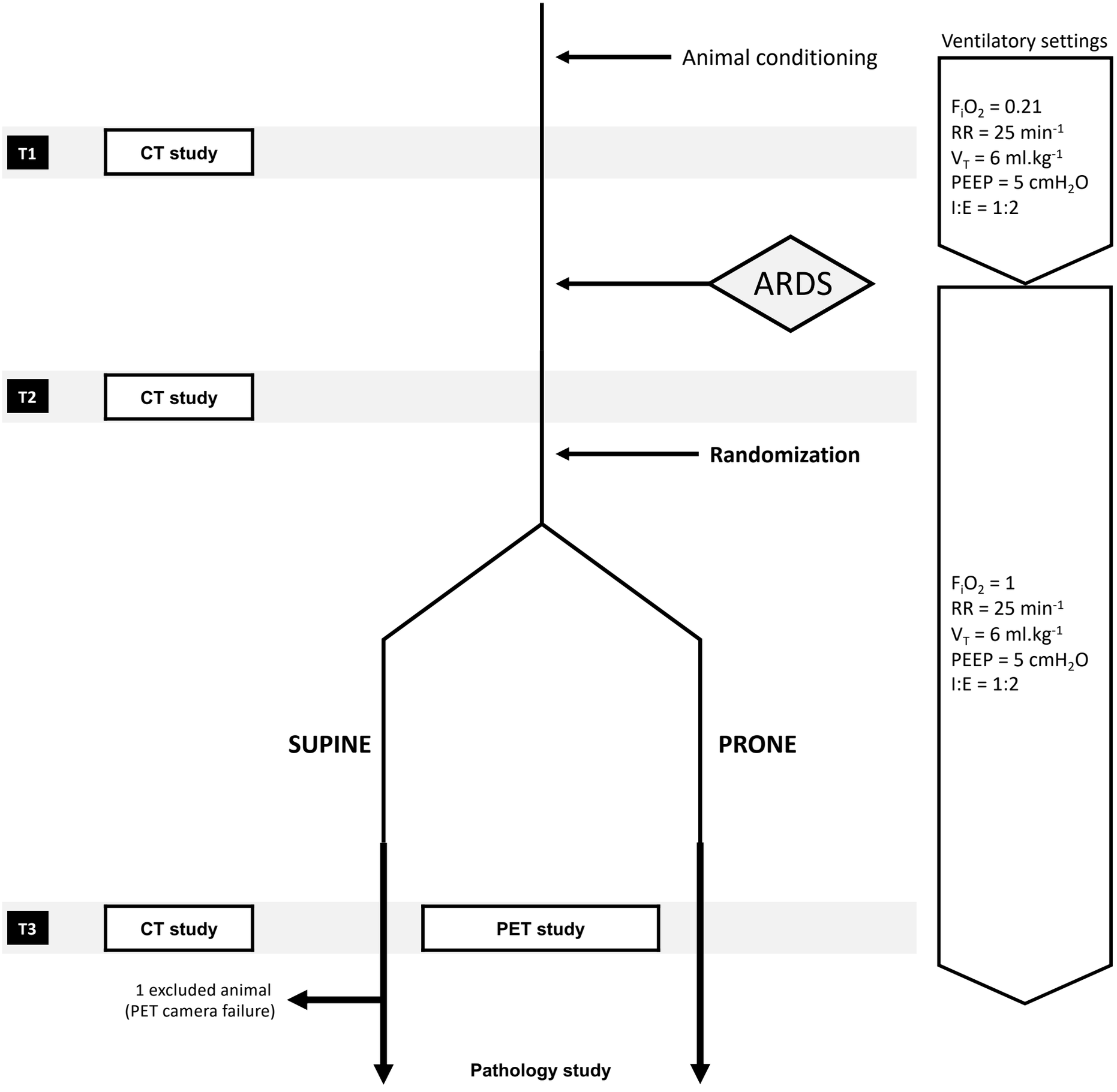
Animal conditioning
Ventilatory settings
F_iO_2 = 0.21
RR = 25 min^{-1}
V_T = 6 $ml.kg^{-1}$
PEEP = 5 cmH_2O
I:E = 1:2
T1
CT study
ARDS
T2
CT study
Randomization
F_iO_2 = 1
RR = 25 min^{-1}
V_T = 6 $ml.kg^{-1}$
PEEP = 5 cmH_2O
I:E = 1:2
SUPINE
PRONE
T3
CT study
PET study
1 excluded animal
(PET camera failure)
Pathology study

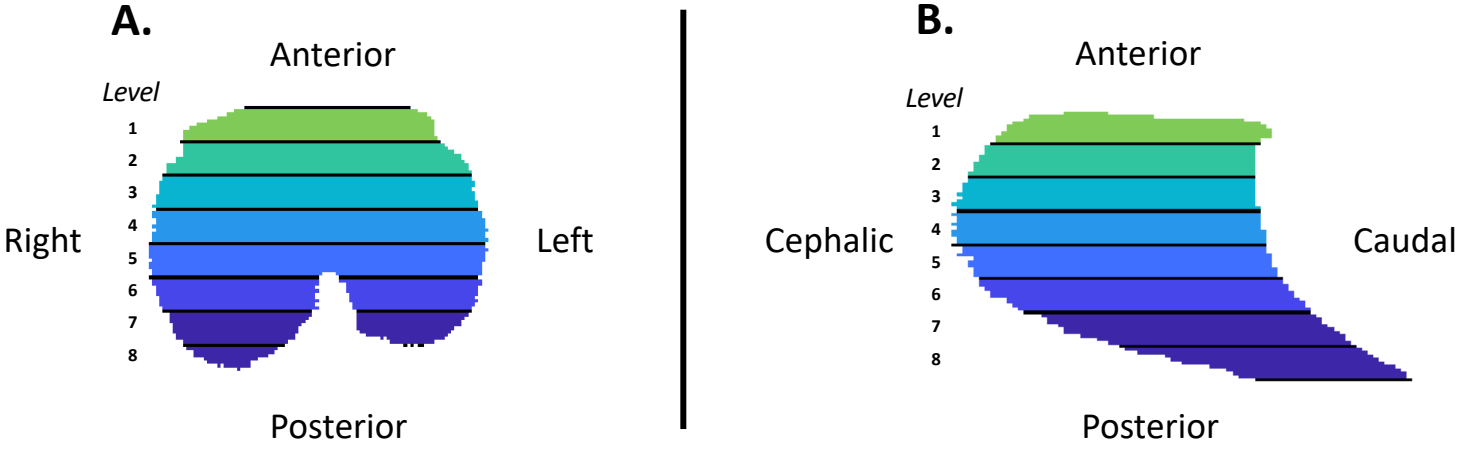
A.
Anterior
Level
1
2
3
4
5
6
7
8
Right
Left
Posterior
B.
Anterior
Level
1
2
3
4
5
6
7
8
Cephalic
Caudal
Posterior

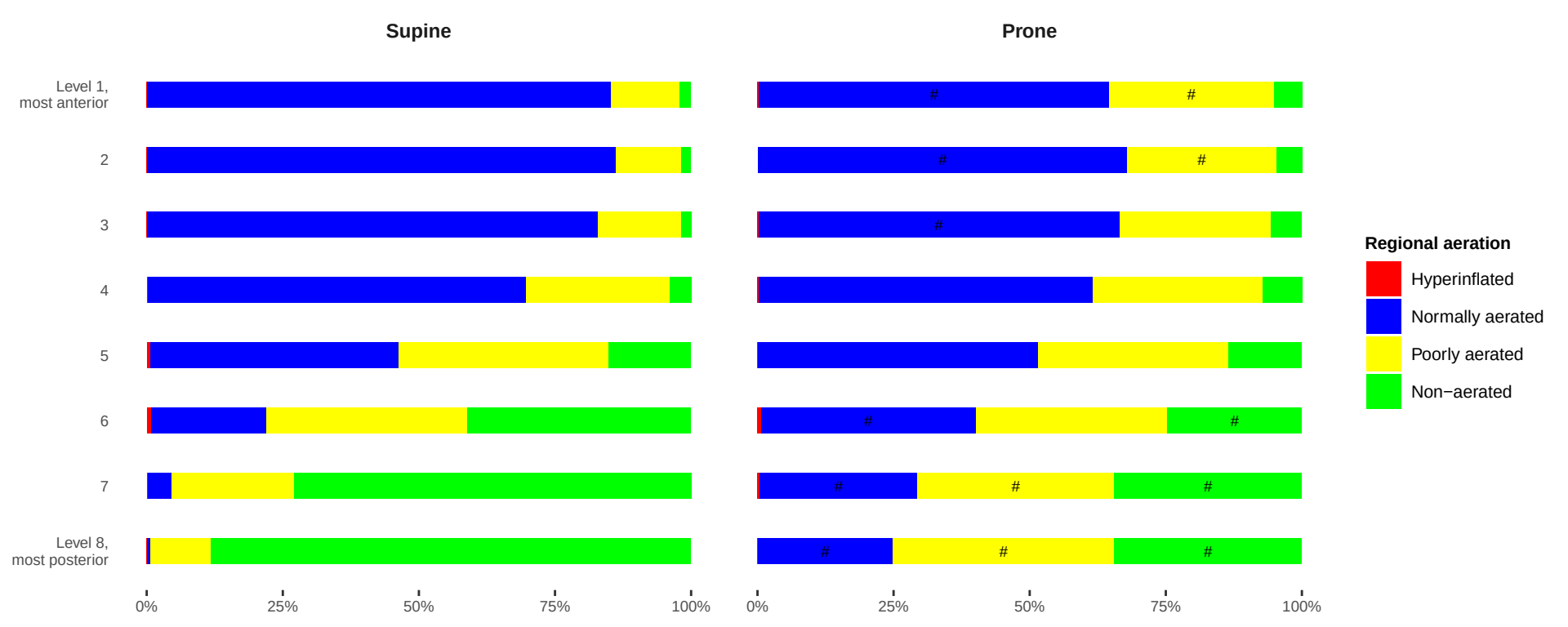
Supine
Prone
Level 1, most anterior
2
3
4
5
6
7
Level 8, most posterior
0%
25%
50%
75%
100%
Regional aeration
Hyperinflated
Normally aerated
Poorly aerated
Non−aerated

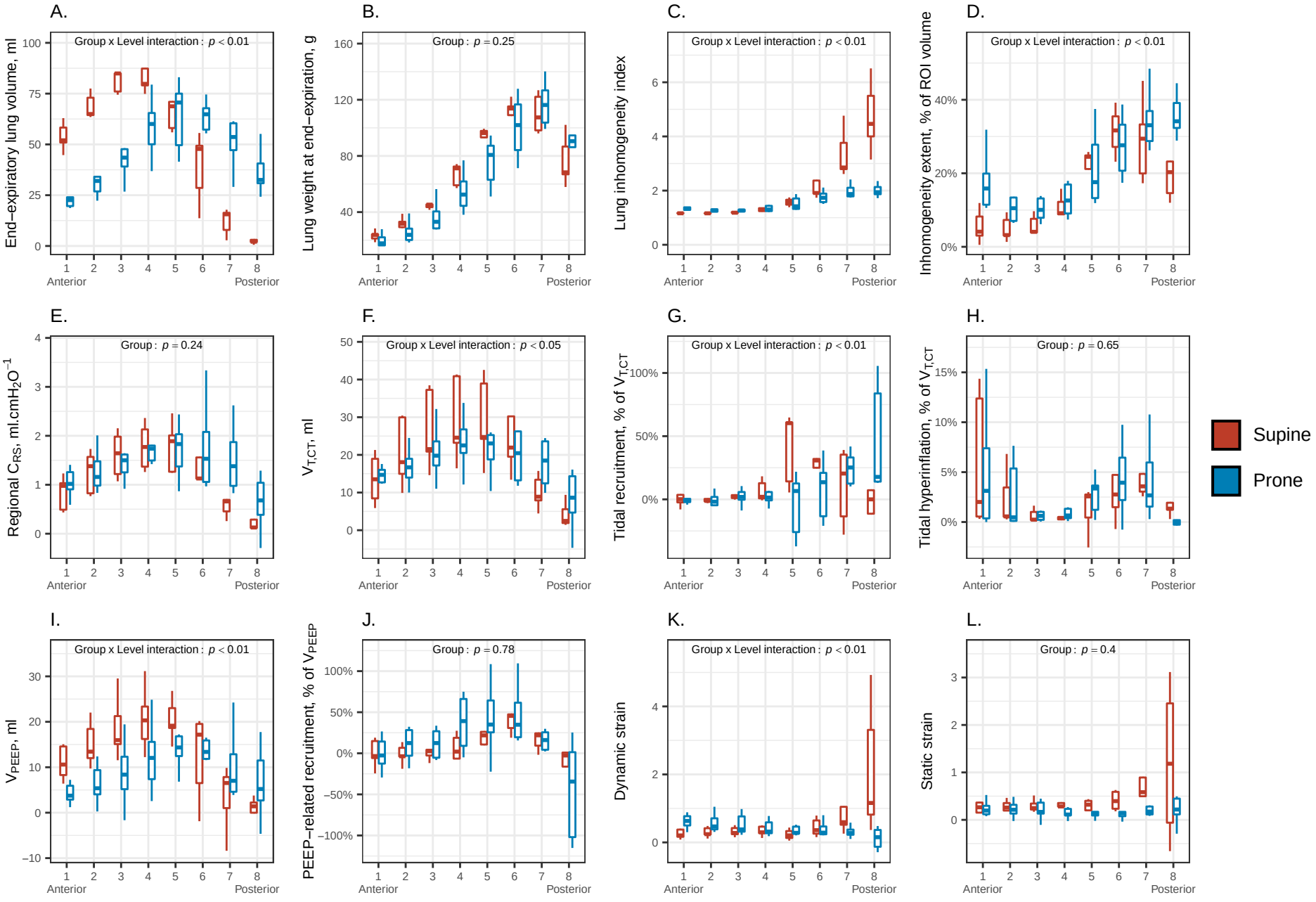
A.
End–expiratory lung volume, ml
Group x Level interaction : p < 0.01
B.
Lung weight at end–expiration, g
Group : p = 0.25
C.
Lung inhomogeneity index
Group x Level interaction : p < 0.01
D.
Inhomogeneity extent, % of ROI volume
Group x Level interaction : p < 0.01
E.
Regional C_RS, ml.cmH2O^-1
Group : p = 0.24
F.
V_T,CT, ml
Group x Level interaction : p < 0.05
G.
Tidal recruitment, % of V_T,CT
Group x Level interaction : p < 0.01
H.
Tidal hyperinflation, % of V_T,CT
Group : p = 0.65
I.
V_PEEP, ml
Group x Level interaction : p < 0.01
J.
PEEP–related recruitment, % of V_PEEP
Group : p = 0.78
K.
Dynamic strain
Group x Level interaction : p < 0.01
L.
Static strain
Group : p = 0.4
Anterior
Posterior
Supine
Prone
Antero-posterior lung levels

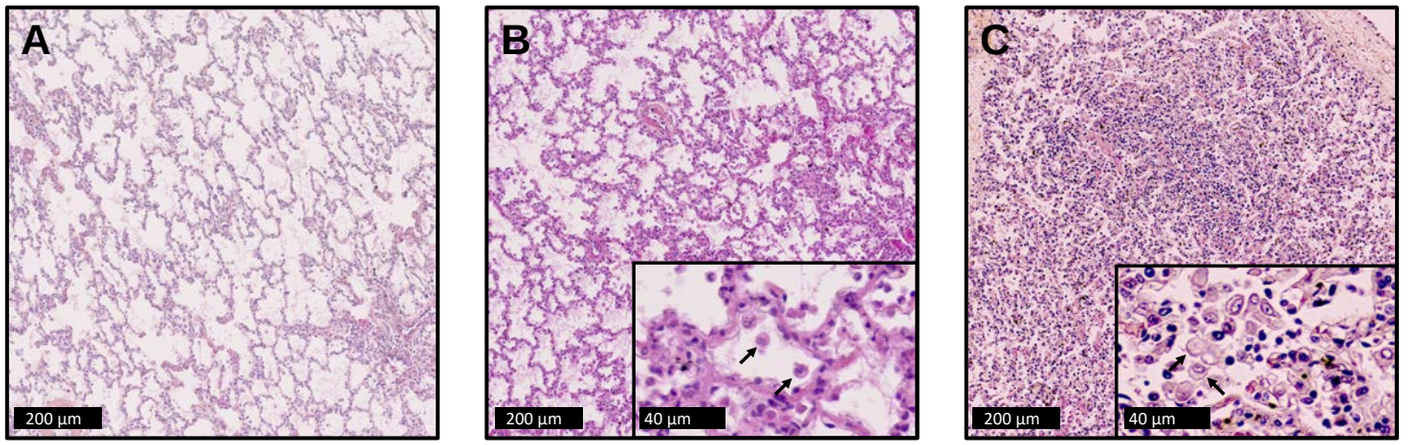

Antero-medial lung region
Normal lung
Macrophage score = 0

Antero-caudal lung region
Mild macrophage recruitment
Macrophage score = 1

Postero-caudal lung region
Moderate macrophage recruitment,
Macrophage score = 2

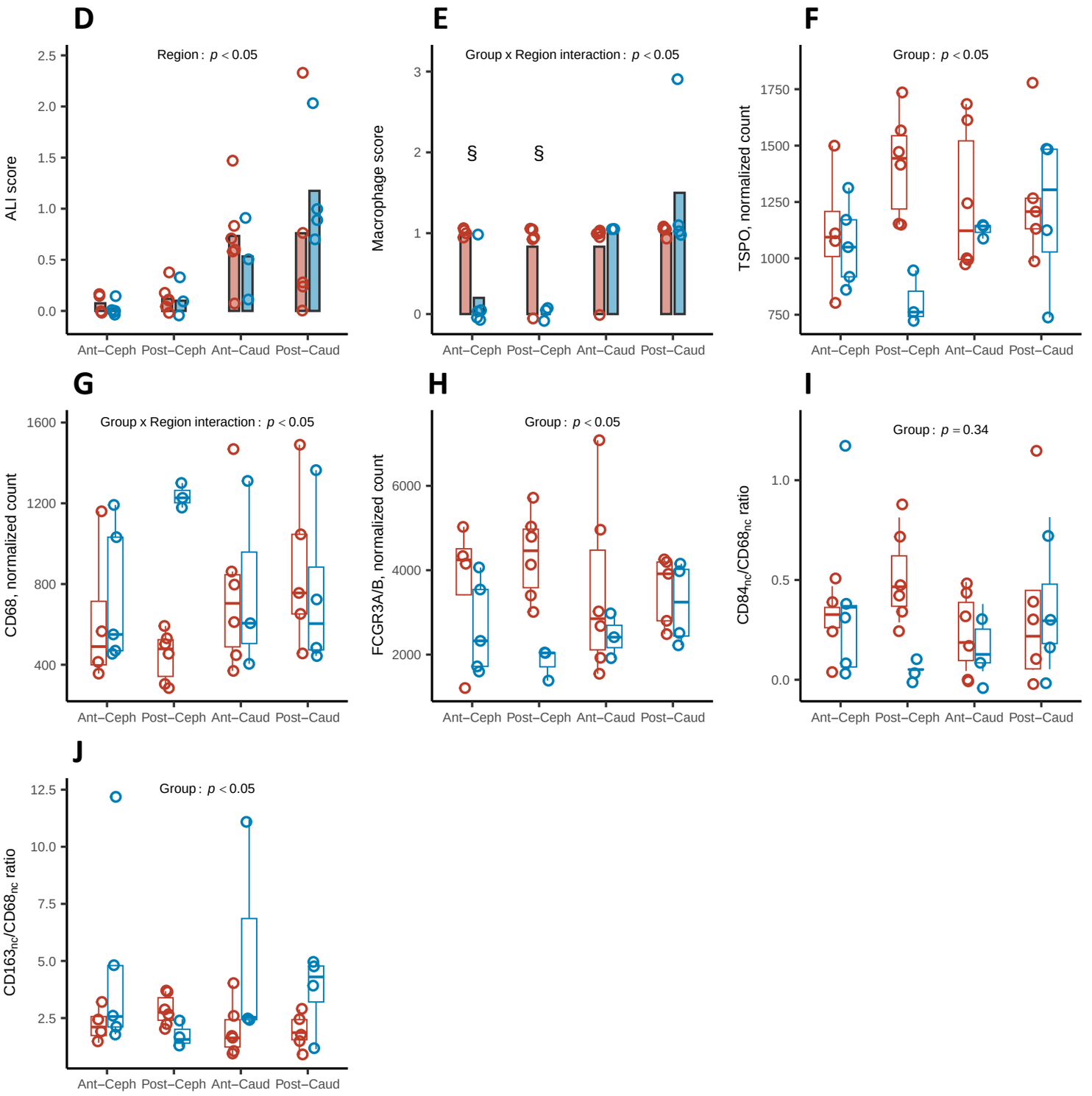

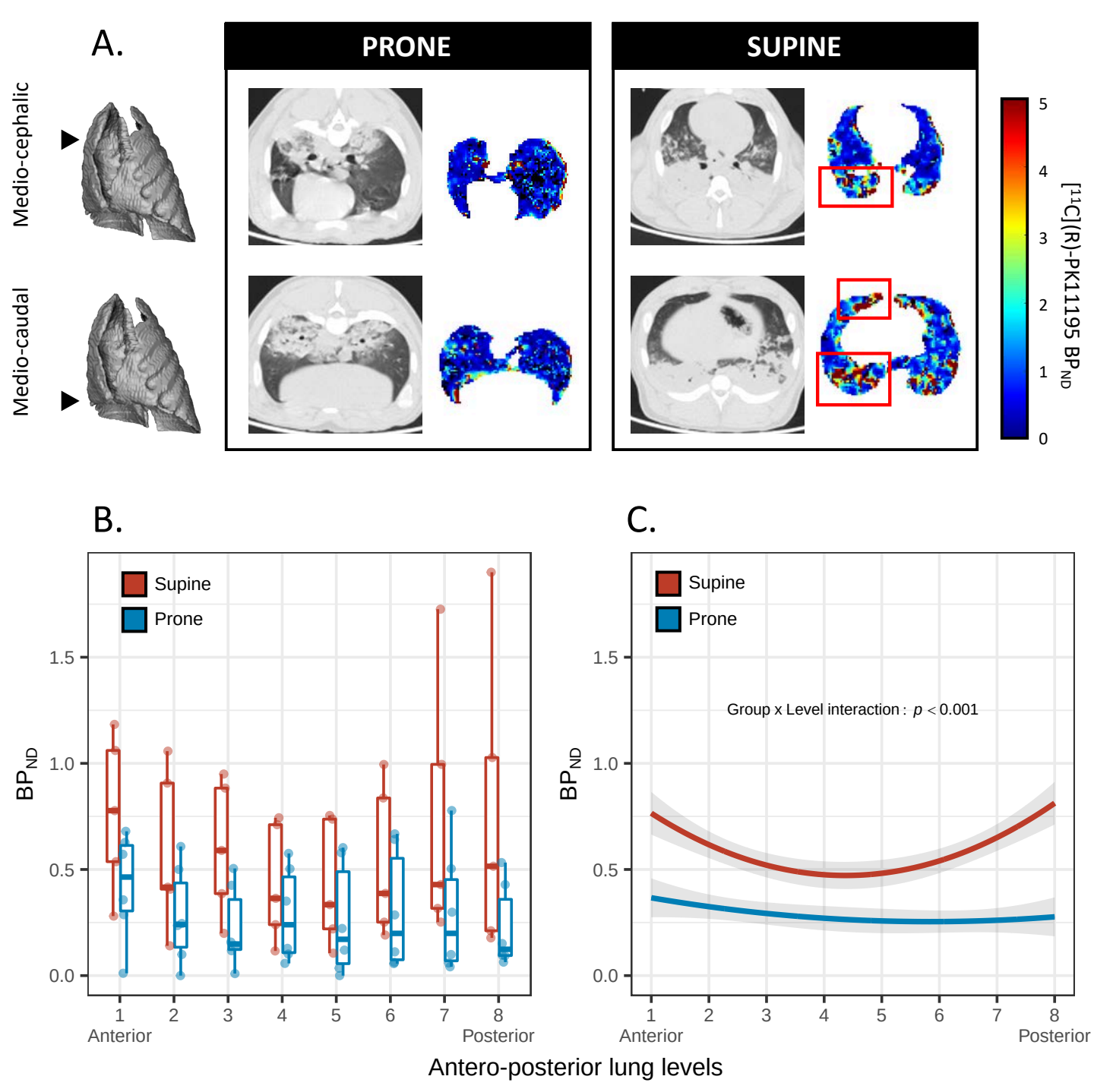
A.
PRONE
SUPINE
Medio-cephalic
Medio-caudal
[11C](R)-PK11195 BPND
5
4
3
2
1
0
B.
Supine
Prone
BPND
1.5
1.0
0.5
0.0
1
2
3
4
5
6
7
8
Anterior
Posterior
C.
Supine
Prone
Group x Level interaction : p < 0.001
BPND
1.5
1.0
0.5
0.0
1
2
3
4
5
6
7
8
Anterior
Posterior
Antero-posterior lung levels

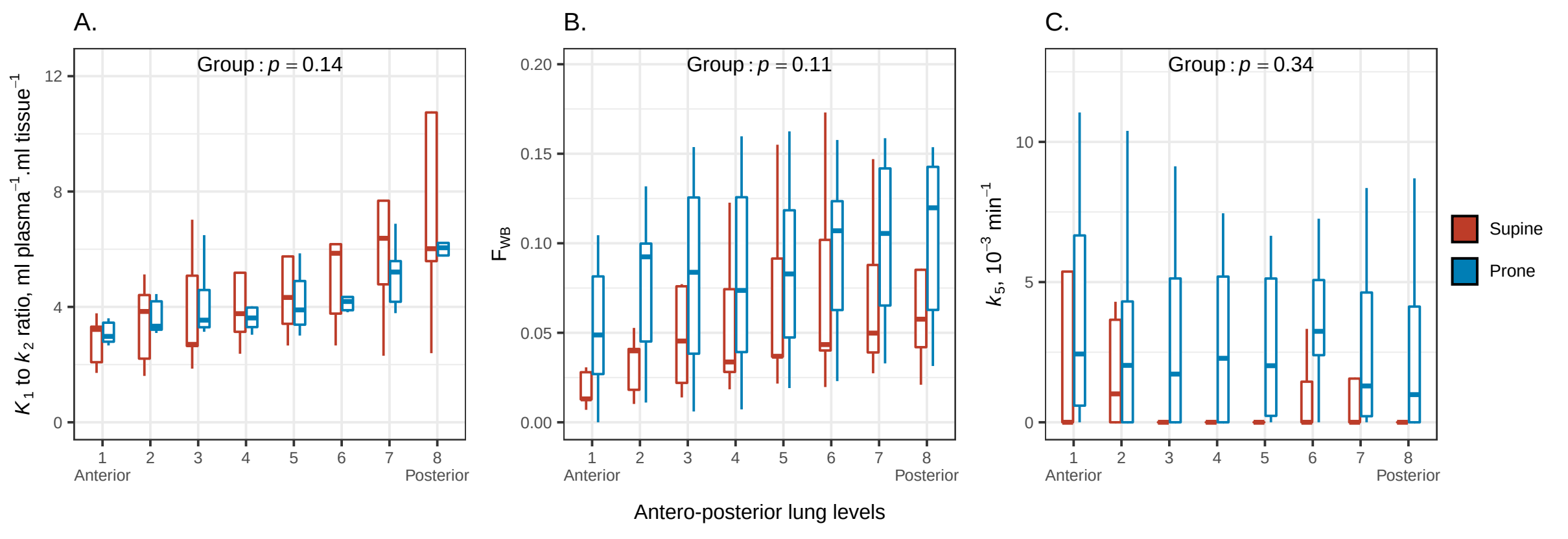
A.
B.
C.
Group : $p = 0.14$
Group : $p = 0.11$
Group : $p = 0.34$
K_1 to k_2 ratio, ml plasma^{-1}.ml tissue^{-1}
F_{WB}
k_5, 10^{-3} min^{-1}
Anterior
Posterior
Antero-posterior lung levels
Supine
Prone

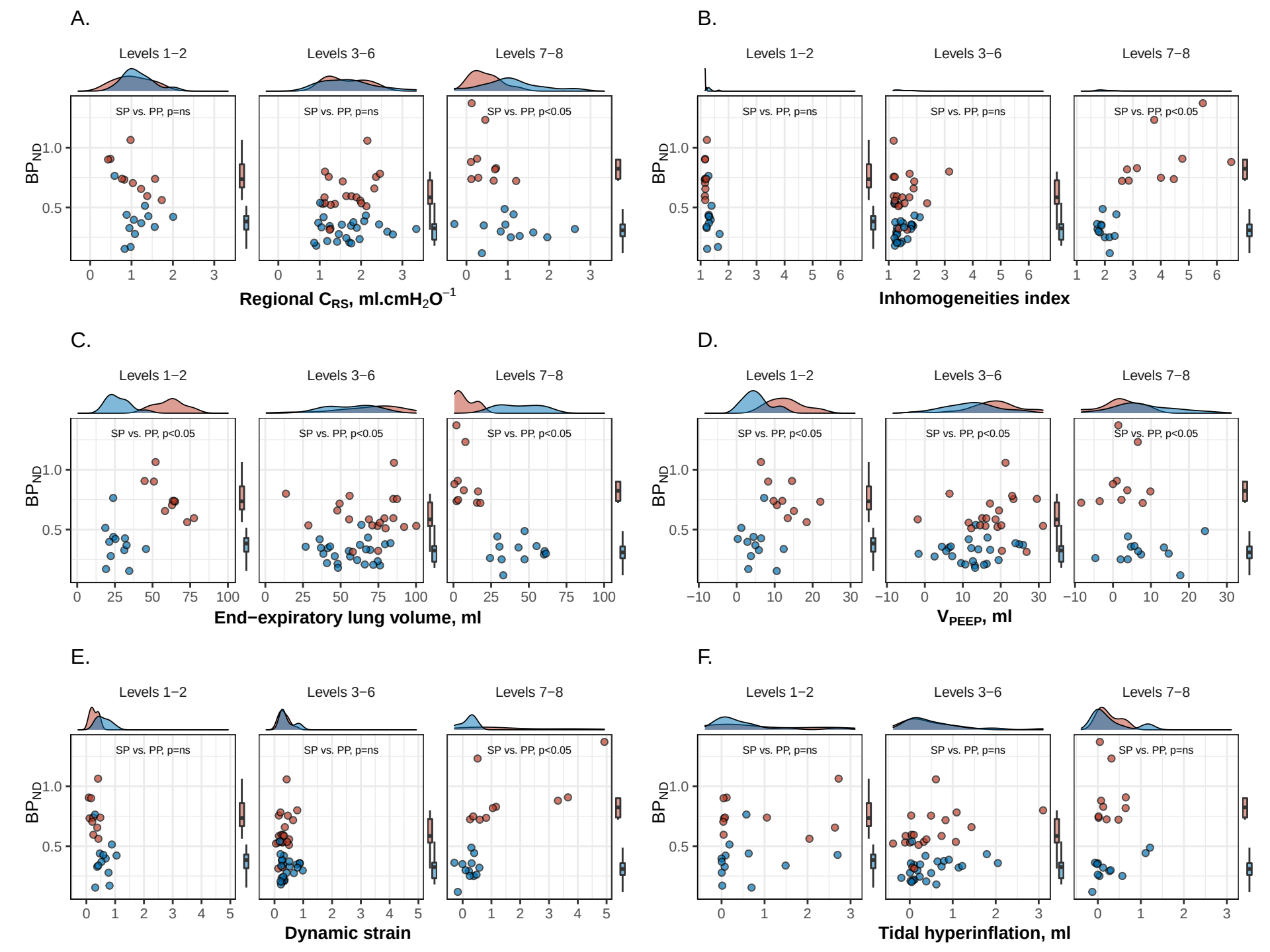
A.
Levels 1−2
Levels 3−6
Levels 7−8
SP vs. PP, p=ns
SP vs. PP, p=ns
SP vs. PP, p<0.05
BPND
Regional CRS, ml.cmH2O−1
B.
Levels 1−2
Levels 3−6
Levels 7−8
SP vs. PP, p=ns
SP vs. PP, p=ns
SP vs. PP, p<0.05
BPND
Inhomogeneities index
C.
Levels 1−2
Levels 3−6
Levels 7−8
SP vs. PP, p<0.05
SP vs. PP, p<0.05
SP vs. PP, p<0.05
BPND
End−expiratory lung volume, ml
D.
Levels 1−2
Levels 3−6
Levels 7−8
SP vs. PP, p<0.05
SP vs. PP, p<0.05
SP vs. PP, p<0.05
BPND
VPEEP, ml
E.
Levels 1−2
Levels 3−6
Levels 7−8
SP vs. PP, p=ns
SP vs. PP, p=ns
SP vs. PP, p<0.05
BPND
Dynamic strain
F.
Levels 1−2
Levels 3−6
Levels 7−8
SP vs. PP, p=ns
SP vs. PP, p=ns
SP vs. PP, p=ns
BPND
Tidal hyperinflation, ml

Table 1. Respiratory mechanics over time

Variables | *study time points*	**Study group**		**Effect of group, *p***	**Effect of time, *p***	**Group × time, *p***
	Supine n=5	**Prone n=6**			
Tidal volume, $ml.kg^{-1}$			>0.99	>0.99	>0.99
T1	6 [5.9–6.1]	5.9 [5.9–6]			
T2	6 [5.9–6.1]	5.9 [5.9–6]			
T3	6 [5.9–6.1]	5.9 [5.9–6]			
Respiratory rate, $breaths.min^{-1}$			0.07	>0.99	>0.99
T1	25 [25–25]	25 [25–25]			
T2	25 [25–25]	25 [25–25]			
T3	25 [25–25]	25 [25–25]			
Plateau pressure, cmH_2O			-	-	0.01
T1	14 [12–14]	12 [12–12]			
T2	23 [21–24]†	20 [19–22]†			
T3	24 [19–25]†	18 [18–19]†,‡			
Total PEEP, cmH_2O			0.01	0.73	0.75
T1	6 [6–6]	6 [5–6]			
T2	7 [6–7]	6 [6–6]			
T3	6 [6–6]	5 [5–6]			
ΔP_{AW}, cmH_2O			0.14	<0.01	0.06
T1	7 [6–7]	7 [6–7]			
T2	17 [15–18]	14 [13–17]		*	
T3	17 [13–19]	13 [12–14]		*	
$\Delta P_{ES,}$ cmH_2O			-	-	0.01
T1	2 [1–2]	2 [2–2]			
T2	2 [2–3]	3 [2–3]			
T3	3 [2–3]	4 [3–4]†,‡			
El_{RS}, $cmH_2O.L^{-1}$			0.32	<0.01	0.14
T1	43 [33–44]	41 [37–41]			
T2	94 [94–100]	96 [77–100]		*	
T3	90 [86–96]	78 [74–87]		*	
El_{CW}, $cmH_2O.L^{-1}$			-	-	0.01
T1	10 [8–11]	13 [10–14]			
T2	15 [10–16]	20 [11–21]			
T3	14 [11–17]	24 [21–25]†,‡			
El_{L}, $cmH_2O.L^{-1}$			-	-	0.01
T1	33 [23–36]	28 [24–30]			
T2	84 [73–93]†	76 [59–89]†			
T3	79 [76–79]†	56 [52–63]†,‡			
$P_{L,EI}$, cmH_2O			-	-	<0.01
T1	10 [9–10]	9 [7–9]			
T2	20 [19–21]†	16 [15–18]†			
T3	19 [17–22]†	13 [12–13]†,‡			
Elastic mechanical power, $J.min^{-1}$			-	-	0.02
T1	3.9 [3.1–5.3]	3.6 [3.1–3.7]			
T2	5.6 [5.3–8.2]†	5.0 [4.7–5.2]†			
T3	6.0 [5.0–7.9]†	4.8 [4.4–5.1]†			

Values are median with interquartile range. Study time points were baseline (T1, normal lungs), after experimental ARDS stabilization period (T2), and 4h later (T3). The analysis used all data collected in both groups at the 3 study time points, using a mixed effects linear regression with study group and study time point as independent variables, and animal identification number as the random effect. Interaction of time with study group was systematically checked for. If no interaction was identified, the p values of the effect of Group and Time are given, respectively. In case of a significant interaction, a pairwise post-hoc multiple comparison was performed to compare groups at each time point on the one side, and compare T2 and T3 to T1 in each group, on the other. Multiple comparisons were adjusted for α inflation using the Tukey method. *: p<0.05 compared to T1 at the time point (no interaction with study group); †: p<0.05 compared to T1 in this study group; ‡: p<0.05 compared to the supine group at this time point. ΔP_{AW}: difference in airway pressure at end-inspiration (plateau pressure) and end-expiration (total PEEP); ΔP_{ES}: difference in esophageal pressure at end-inspiration and end-expiration; $P_{L,EI}$: elastance-

derived plateau transpulmonary pressure; El_{CW}: chest wall elastance; El_{L}: lung elastance; El_{RS}: respiratory system elastance; PEEP: positive end-expiratory pressure.

Table 2. Computed tomography-derived parameters over time

Variables (whole lung) | *study time points*	**Supine n=5**	**Prone n=6**	**Effect of group, *p***	**Effect of time, *p***	**Group × time, *p***
Lung tissue weight at end-expiration, g			0.62	<0.01	0.83
T1	477 [420–503]	442 [407–475]			
T2	568 [512–625]	510 [501–571]		*	
T3	599 [559–621]	565 [544–588]		*	
End-expiratory non-aerated lung volume, ml			-	-	0.03
T1	47 [28–54]	44 [39–50]			
T2	190 [185–205]†	190 [152–225]†			
T3	272 [213–294]†	178 [144–207]†,‡			
End-expiratory aerated lung volume (EELV), ml			0.77	<0.01	0.09
T1	607 [545–622]	602 [599–628]			
T2	458 [441–476]	475 [382–566]		*	
T3	430 [408–472]	393 [359–434]		*	
Gas fraction at end-expiration			0.95	<0.01	0.42
T1	0.56 [0.53–0.57]	0.57 [0.56–0.59]			
T2	0.45 [0.42–0.47]	0.44 [0.42–0.47]		*	
T3	0.42 [0.39–0.45]	0.41 [0.37–0.43]		*	
Tidal volume ($V_{T,CT}$), ml.kg^{-1}			0.66	0.65	0.73
T1	5.6 [5.4–6.5]	5.5 [5.4–5.6]			
T2	5.7 [5.7–6.4]	5.4 [4.9–5.8]			
T3	6.1 [5.0–6.4]	5.9 [5.6–6.2]			
Tidal recruitment, ml			0.87	0.04	0.59
T1	13 [5–26]	0 [-1–3]			
T2	23 [9–42]	29 [20–40]			
T3	30 [27–43]	25 [19–34]		*	
Tidal hyperinflation, ml			>0.99	0.10	0.73
T1	1 [1–2]	2 [2–3]			
T2	3 [3–4]	4 [2–6]			
T3	3 [1–8]	4 [3–4]			
PEEP-related increase in gas volume (V_{PEEP}), ml			0.06	<0.01	0.30
T1	150 [147–169]	138 [130–157]			
T2	125 [101–131]	93 [85–94]§			
T3	109 [106–112]	77 [67–92]		*	
PEEP-related alveolar recruitment, ml			0.07	0.91	0.99
T1	18 [5–35]	2 [0–4]			
T2	14 [13–23]	3 [-3–29]§			
T3	18 [17–20]	11 [7–14]			
Dynamic strain			0.95	0.50	0.14
T1	0.22 [0.22–0.35]	0.26 [0.25–0.31]			
T2	0.33 [0.23–0.33]	0.23 [0.21–0.24]			
T3	0.28 [0.21–0.37]	0.34 [0.30–0.36]			
Static strain			0.82	0.06	0.92
T1	0.28 [0.25–0.29]	0.28 [0.26–0.29]			
T2	0.31 [0.20–0.31]	0.15 [0.11–0.28]§			
T3	0.23 [0.21–0.23]	0.20 [0.15–0.30]			
Index of lung inhomogeneity at end-expiration			0.78	<0.01	0.78
T1	1.30 [1.26–1.31]	1.27 [1.26–1.29]			
T2	1.53 [1.50–1.69]	1.58 [1.49–1.68]		*	
T3	1.63 [1.56–1.68]	1.63 [1.57–1.74]		*	
Extent of lung inhomogeneity at end-expiration			-	-	<0.01
T1	0.12 [0.11–0.15]	0.11 [0.10–0.11]			
T2	0.22 [0.15–0.23]†	0.17 [0.17–0.18]†			
T3	0.15 [0.15–0.20]	0.24 [0.22–0.30]†,‡			

Values are median with interquartile range. Study time points were baseline (T1, normal lungs), after experimental ARDS stabilization period (T2), and 4h later (T3). The analysis used all data collected in both groups at the 3 study time points, using a mixed effects linear regression with study group and study time point as independent variables, and animal identification number as the random effect. Interaction of time with study group was systematically checked for. If no interaction was identified, the p values of the effect of Group and Time are given, respectively. In case of a significant interaction, a pairwise post-hoc multiple comparison was performed to compare groups at each time point on the one side, and compare T2 and T3 to T1 in each group, on the other. Multiple comparisons were adjusted for α inflation using the Tukey method. *: p<0.05 compared to T1 at the time point (no interaction with study group); †: p<0.05 compared to T1 in this study group; ‡: p<0.05 compared to the supine group at this time point; §: no test was performed due to missing values at

this time point. EELV: end-expiratory aerated lung volume; V_{PEEP}: PEEP-related increase in gas volume; $V_{T,CT}$: computerized tomography-derived tidal volume

Table 3. Association of regional CT parameters with regional BP_{ND}

	Univariate analysis		*Multivariate analysis*	
Regional variables (88 measurements)	**Regional BP_{ND}** β±SE	***p***	**Regional BP_{ND}** β±SE	***p***
Study group: supine position (reference is prone)	0.20±0.12	0.10	0.35±0.13	0.03
Non-aerated lung volume at end-expiration, per 10 ml increase	0.02±0.01	0.08	*nr*	
End-expiratory lung volume, per 10 ml increase	-0.03±0.01	0.01	*mc*	
End-expiratory tissue fraction, per 0.1 increase	-0.01±0.01	0.54	*ns*	
Tidal volume, per 10 ml increase	-0.06±0.02	<0.01	*mc*	
Tidal recruitment, per 1 ml increase	-0.01±0.004	0.03	*nr*	
Tidal hyperinflation, per 1 ml increase	0.04±0.03	0.18	0.06±0.03	<0.05
PEEP-related increase in gas volume (V_{PEEP}), per 10 ml increase	-0.06±0.04	0.04	*nr*	
PEEP-related alveolar recruitment, per 10 ml increase	-0.05±0.04	0.18	*nr*	
Regional C_{RS}, per 1 ml.cmH_2O^{-1} increase	-0.08±0.03	0.01	-0.07±0.03	0.01
Dynamic strain, per 1 unit increase	0.09±0.03	<0.01	0.10±0.03	<0.01
Static strain, per 1 unit increase	0.02±0.02	0.30	*ns*	
Lung inhomogeneity index, per 1 unit increase	0.09±0.03	0.01	*mc*	
Lung inhomogeneity extent, per 10% increase	-0.02±0.02	0.41	*ns*	

Variables with a *p* value ≤ 0.20 were included in the multivariate analysis. All continuous variables were scaled and centered prior to regression, and their coefficients back-scaled subsequently. Multicollinearity and interactions of variables were systematically checked for. Variables with a VIF > 3 were excluded before the backward stepwise selection of variables and are identified by Ø in the multivariate analysis column when present. Significance of the multivariate model was evaluated using bootstrap with 500 simulations. Model residuals were checked graphically for normality. The final model marginal R^2 was 0.27 and had a conditional R^2 of 0.87. *nr*: included in the multivariate model, but not retained in the final model after backward stepwise selection; *mc*: excluded from the multivariate model due to multicollinearity (VIF > 3); *ns*: variable excluded from the multivariate analysis (*p* > 0.20). β: model coefficient; BP_{ND}: [^{11}C](R)-PK11195 binding potential; C_{RS}: respiratory system compliance; PEEP: positive end-expiratory pressure; SE: standard error; VIF: variance inflation factor; V_{PEEP}: PEEP-related increase in gas volume.